

DESIGN OF A SMALL SOLAR-POWERED UNMANNED AERIAL VEHICLE

A Thesis

Presented to

The Faculty of the Department of Mechanical and Aerospace Engineering

San José State University

In Partial Fulfillment

of the Requirements for the Degree

Master of Science

by

Christopher J. Hartney

August 2011

© 2011

Christopher J. Hartney

ALL RIGHTS RESERVED

The Designated Thesis Committee Approves the Thesis Titled

DESIGN OF A SMALL SOLAR-POWERED UNMANNED AERIAL VEHICLE

By

Christopher J. Hartney

APPROVED FOR THE DEPARTMENT OF MECHANICAL AND AEROSPACE
ENGINEERING

SAN JOSÉ STATE UNIVERSITY

August 2011

Dr. Nikos Mourtos	Department of Mechanical and Aerospace Engineering
Dr. Periklis Papadopoulos	Department of Mechanical and Aerospace Engineering
Dr. James Mokri	Department of Mechanical and Aerospace Engineering

ABSTRACT

DESIGN OF A SMALL SOLAR-POWERED UNMANNED AERIAL VEHICLE

By Christopher J. Hartney

This thesis studies a conceptual design of a solar-powered unmanned aerial vehicle (UAV) that has a wingspan no more than 7 m and a mass of less than 10 kg, 2.27 kg are devoted to payload. This UAV will be used specifically to study wildfires in California and will have the necessary equipment needed for such a mission, including a Global Positioning System (GPS) and cameras. A weight analysis and a power sensitivity analysis were researched, and it was shown that this aircraft will generate 350 W of power – 114.6 W greater than the power available to fly. Also, a stability and controls analysis was done and the required tail area that is needed for stability was calculated. Using XFRL5, a drag polar estimation was calculated and compared with Roskam's methods to prove accuracy of results.

ACKNOWLEDGEMENTS

This thesis could never have been completed without the endless support of my committee members, friends and family.

First, I would like to thank Professor Nikos Mourtos for his technical guidance and knowledge of aircraft design. Throughout my research, he supported me, and provided me with more unique opportunities than I thought I would ever experience. Without him, this thesis would not have been possible.

Second, I wish to thank Professor Periklis Papadopoulos for his opinions and recommendations. Throughout my graduate studies research, he has provided me with help whenever needed and has broadened my knowledge and technical expertise in the field of astrodynamics.

Third, I would like to thank Professor James Mokri for his solar technology advice when it came to choosing the components for this aircraft. Without him, my knowledge of solar cell technology would be limited.

Finally, to all my friends and family, thank you for supporting me throughout my lifetime. Stephanie, you have been there for me these last few years and have dramatically improved every aspect of my life, and I love you very much. Dad, you were there whenever I needed someone to talk to during my early life, and you have been a great father and friend to me. Finally, to my mom: you have been my driving motivation throughout my college career. You are the reason why I have an endless drive to succeed. You will always be in my heart for the rest of my life. I miss you very much.

To receive a master's degree is a great honor, but being the first member of my family to be rewarded with a master's degree is even a greater honor. Again, thank you very much to everyone who has supported me throughout my lifetime.

TABLE OF CONTENTS

LIST OF FIGURES	xii
LIST OF TABLES.....	xiii
LIST OF SYMBOLS	xiv
1.0 INTRODUCTION	1
1.1 MOTIVATION.....	1
1.2 OBJECTIVES.....	1
1.3 LITERATURE REVIEW	2
1.3.1 History of Solar-Powered Flight.....	2
1.3.2 Other UAV Studies.....	5
1.3.3 Future Considerations	6
2.0 MISSION SPECIFICATION.....	6
2.1 MISSION REQUIREMENTS	6
2.1.1 Payload	6
2.1.2 Crew Members Required	7
2.1.3 Range / Endurance	7
2.1.4 Cruise Speed	7
2.1.5 Cruise Altitude.....	7
2.1.6 Take-off and Landing	7
2.2 MISSION PROFILE.....	8
2.3 MARKET ANALYSIS.....	9
2.4 TECHNICAL AND ECONOMIC FEASIBILITY	9
2.5 CRITICAL MISSION REQUIREMENTS.....	10

3.0 COMPARATIVE STUDY OF SIMILAR AIRPLANES.....	10
3.1 MISSION CAPABILITIES AND CONFIGURATION SLECTION.....	10
3.2 COMPARISON OF IMPORTANT DESIGN PARAMETERS	13
4.0 COMPARATIVE STUDY OF AIRPLANES WITH SIMILAR MISSION PERFORMANCE.....	14
5.0 SELECTION OF PROPULSION SYSTEM	15
5.1 SELECTION OF THE PROPULSION SYSTEM TYPE.....	15
5.2 SELECTION OF THE NUMBER OF ENGINES.....	15
5.3 PROPELLER SIZING.....	15
6.0 CONFIGURATION SELECTION.....	16
6.1 OVERALL CONFIGURATION.....	16
6.2 WING CONFIGURATION.....	16
6.3 EMPENNAGE CONFIGURATION	20
6.4 LANDING GEAR DISPOSITION.....	21
6.5 PROPOSED CONFIGURATION	21
7.0 MISSION WEIGHT ESTIMATES	22
7.1 COMMENTS.....	22
7.2 DATABASE FOR WEIGHTS OF SIMILAR AIRCRAFT	23
7.3 DETERMINATION OF MISSION WEIGHTS	23
7.3.1 Determination of Power Available	24
7.3.2 Fixed Masses	25
7.3.3 Mass of Airframe.....	25
7.3.4 Mass of Solar Cells.....	25
7.3.5 Mass of Maximum Power Point Tracker	26

7.3.6 Mass of Batteries	26
7.3.7 Mass of Propulsion Group	27
7.3.8 Results	27
8.0 PERFORMANCE CONSTRAINT ANALYSIS	29
8.1 COMMENTS.....	29
8.2 SIZING TO CRUISE SPEED REQUIREMENTS	30
8.3 SIZING TO FAR 23 RATE OF CLIMB REQUIREMENTS.....	31
8.4 PERFORMANCE SIZING GRAPH	32
8.5 POWER ANALYSIS.....	34
8.5 STALL SPEED.....	35
9.0 FUSELAGE DESIGN	36
10.0 WING, HIGH LIFT SYSTEM, AND LATERAL CONTROLS DESIGN	37
10.1 WING PLANFORM DESIGN	37
10.2 TAPER RATIO	37
10.3 DIHEDRAL ANGLE	37
10.4 INCIDENCE ANGLE	38
10.5 AIRFOIL SELECTION.....	38
10.6 HIGH LIFT DEVICES	38
10.7 CONTROL SURFACES	38
10.8 WING CAD DRAWING.....	39
11.0 EMPENNAGE DESIGN AND CONTROLS ANALYSIS.....	39
11.1 OVERALL EMPENNAGE DESIGN.....	39
11.2 EMPENNAGE AIRFOIL	41

11.3 OTHER EMPENNAGE PARAMETERS	44
11.4 DESIGN OF THE LONGITUDINAL AND DIRECTIONAL CONTROLS.....	44
11.5 EMPENNAGE CAD DRAWINGS.....	45
11.6 COMPLETE AIRCRAFT CAD DRAWINGS.....	45
12.0 WEIGHT AND BALANCE	45
12.1 COMPONENT WEIGHT BREAKDOWN	45
12.2 CENTER OF GRAVITY CALCULATIONS AND DISCUSSION	50
13.0 STABILITY AND CONTROL ANALYSIS.....	54
13.1 STATIC LONGITUDINAL STABILITY	54
13.2 STATIC DIRECTIONAL STABILITY	58
14.0 DRAG POLAR ESTIMATION.....	60
14.1 AIRPLANE ZERO LIFT DRAG.....	60
14.2 AIRPLANE DRAG POLAR	62
14.3 DISCUSSION.....	64
15.0 ENVIRONMENTAL / ECONOMIC TRADEOFFS.....	65
15.1 ENVIRONMENTAL ISSUES	65
15.2 ECONOMIC TRADEOFFS	66
15.3 SOLUTIONS	67
16.0 CONCLUSIONS / RECOMMENDATIONS.....	67
REFERENCES	68
APPENDICES	70
Appendix A: Complete Design Parameters for Similar Aircraft	70
Appendix B: Front, Side, and Top Views for Initial Configuration.....	71

Appendix C: Matlab M-Files for Solar-Powered Aircraft Analysis	73
Appendix C.1: InitParameters2.m.....	73
Appendix C.2: EvaluateSolution.m	75
Appendix C.3: Function MinimumPositive.m.....	77
Appendix C.4: Main.m	78
Appendix C.5: Stability and Control Analysis.....	80
Appendix D: Fuselage Drawings.....	83
Appendix E: Main Wing Drawings	85
Appendix F: Empennage Drawings.....	87
Appendix G: Main Aircraft Configuration	89
Appendix H: Other AutoCAD Drawings.....	91
Appendix I: XFLR5 Drag Polar Analysis.....	93

LIST OF FIGURES

Figure 1: Solar-Powered UAV Mission Profile.....	8
Figure 2: Selig 1223 Airfoil with Unit Chord Length	17
Figure 3: XFLR5 Reynolds Number Legend (0.050 is 50000, 0.1 is 100,000, etc.).....	18
Figure 4: Lift-to-Drag Ratio as a Function of Angle of Attack for Selig 1223 Airfoil.....	19
Figure 5: Lift Coefficient as a Function of Angle of Attack for Selig 1223 Airfoil	19
Figure 6: Lift Coefficient as a Function of Drag Coefficient for Selig 1223 Airfoil	20
Figure 7: Moment Coefficient as a Function of Angle of Attack for Selig 1223 Airfoil.....	20
Figure 8: Solar-Powered UAV Proposed Configuration	22
Figure 9: Wingspan versus Mass Distribution.....	28
Figure 10: Proposed Mass and Wingspan.....	28
Figure 11: Correlation between Aircraft Speed and Power Index	31
Figure 12: Performance Sizing Graph	33
Figure 13: NACA 0008 Reynolds Number Legend.....	41
Figure 14: Lift Coefficient versus Drag Coefficient for NACA 0008	42
Figure 15: Lift Coefficient versus Angle of Attack for NACA 0008	42
Figure 16: Moment Coefficient versus Angle of Attack for NACA 0008.....	43
Figure 17: Lift/Drag Ratio versus Angle of Attack for NACA 0008.....	43
Figure 18: Aircraft with Labels	51
Figure 19: Aircraft with Dimensions in Centimeters.....	52
Figure 20: Longitudinal Stability X-Plot	58
Figure 21: Directional Stability X-Plot.....	60

LIST OF TABLES

Table 1: Mission Capabilities for Sunrise I and II, Solar Solitude, and Solar Excel	11
Table 2: Mission Capabilities for SoLong, Zephyr, and SunSailor 1 and 2.....	12
Table 3: Important Design Parameters for Similar Aircraft.....	13
Table 4: Mission Parameters and Calculation of Weight and Wing Loading.....	23
Table 5: Breakdown of Mass Available for Components.....	29
Table 6: Critical Mission Parameters.....	29
Table 7: Aileron Dimensions.....	39
Table 8: Ruddervator Sizing (For One Ruddervator Only)	44
Table 9: Battery Specifications.....	46
Table 10: Component Weights	49
Table 11: Center of Gravity Locations	53
Table 12: Drag Polar Comparison	64

LIST OF SYMBOLS

A	Aspect Ratio
AR	Aspect Ratio
A_{sc}	Solar Cell Area
b	Wingspan
β	Mach Constant
c	Chord Length
C_D	Wing Drag Coefficient
C_{D_0}	Aircraft Clean Zero-Lift Drag Coefficient
C_L	Wing Lift Coefficient
$C_{L_{ah}}$	Horizontal Tail Lift Curve Slope
$C_{L_{av}}$	Vertical Tail Lift Curve Slope
$C_{L_{aw}}$	Wing Lift Curve Slope
$C_{L_{awf}}$	Wing-Fuselage Lift Curve Slope
$C_{n\beta}$	Yaw Sideslip Moment Coefficient
$C_{n\beta f}$	Fuselage Yaw Sideslip Moment Coefficient

$C_{n\beta wf}$	Wing-Fuselage Yaw Sideslip Moment Coefficient
d	Propeller Diameter
d_f	Equivalent Fuselage Diameter
D_f	Equivalent Fuselage Diameter
D_p	Propeller Diameter
e	Oswald Efficiency Factor
ε_h	Horizontal Downwash Gradient
η_{bec}	BEC (Step-down) Efficiency
η_{cbr}	Cambered Efficiency
η_{chrg}	Battery Charging Efficiency
η_{ctrl}	Motor Controller Efficiency
η_{dchrg}	Battery Discharging Efficiency
η_{grb}	Gearbox Efficiency
η_{mot}	Motor Efficiency
η_{mppt}	Maximum Power Point Tracker Efficiency
η_{plr}	Propeller Efficiency

η_{sc}	Solar Cell Efficiency
η_{wthr}	Weather Efficiency
F_L	Fuselage Length
g	Acceleration due to Gravity
I_{max}	Maximum Solar Irradiance
k	Lift Curve Slope Constant
k_{af}	Airframe Constant
k_{bat}	Energy Density of Battery
k_{enc}	Encapsulation Mass Density
k_{mppt}	Mass/Power Ratio of Maximum Power Point Tracker
k_{prop}	Mass/Power Ratio of Propulsion Group
k_{sc}	Solar Cell Mass Density
K_A	Aspect Ratio Constant
K_h	Horizontal Tail Constant
K_n	Factor Accounting for Wing-Fuselage Interference
K_{wf}	Wing-Fuselage Constant

l_f	Fuselage Length
l_n	Fuselage Nose Length
λ_f	Fuselage Length-to-Diameter Ratio
m	Aircraft Total Mass
m_{af}	Airframe Total Mass
m_{av}	Avionics Total Mass
m_{bat}	Batteries Total Mass
m_{fixed}	Fixed Mass
m_{mppt}	Maximum Power Point Tracker Total Mass
m_{pld}	Payload Total Mass
m_{prop}	Propulsion Group Total Mass
m_{sc}	Solar Cells Total Mass
n	Engine Rotational Rate
n_p	Number of Propeller Blades
P_{av}	Power Required for Avionics
P_{bl}	Power Loading Per Blade

P_{electot}	Total Electrical Power Available
P_{lev}	Power Required for Steady Level Flight
P_{max}	Maximum Power per Engine
P_{pld}	Power Required for Payload
ρ	Density of Air
S	Wing Area
$S_{f,s}$	Total Empennage Side Area
S_v	Vertical Tail Area
$S_{\text{wet,e}}$	Empennage Wetted Area
$S_{\text{wet,f}}$	Fuselage Wetted Area
$S_{\text{wet,tot}}$	Total Airplane Wetted Area
$S_{\text{wet,w}}$	Wing Wetted Area
S_{wing}	Wing Area
$\left(\frac{t}{c}\right)_r$	Wing Root Thickness-to-Chord Ratio
T_{day}	Total Day Time
T_{night}	Total Night Time

V	Aircraft Velocity
$(V_{\text{tip}})_{\text{helical}}$	Helical Propeller Velocity
$(V_{\text{tip}})_{\text{static}}$	Static Propeller Velocity
x_1	Sizing Exponent for Wingspan
x_2	Sizing Exponent for Aspect Ratio
\bar{x}_{AC_A}	Aerodynamic Center Location of Aircraft from Tip of Nose, per Chord Length
\bar{x}_{AC_h}	Aerodynamic Center Location of Horizontal Tail from Tip of Nose, per Chord Length
$\bar{x}_{AC_{wf}}$	Aerodynamic Center Location of Wing-Fuselage Combination from Tip of Nose, per Chord Length
x_v	Distance from the Aerodynamic Center of the Vertical Tail to the Aircraft Center of Gravity

1.0 INTRODUCTION

1.1 MOTIVATION

The main motivation behind this thesis comes from the environmental challenges that the world is facing. From global warming to a lack of natural resources, engineers have had to overcome these challenges for the last 50 years. Commercial aircraft currently use several thousand pounds of fuel to complete their flight, causing a negative impact on the atmosphere because of the carbon emissions released. One way to solve this problem is to eliminate the use of jet fuel and find an alternative, such as hydrogen fuel cells. Many companies are looking at bio-fuels for commercial aircraft, but they will also become scarce over time. Solar-powered aircraft not only can be successful, but they can be a solution to current environmental problems and become the future of aviation.

1.2 OBJECTIVES

The primary objective for this report is to design a solar-powered unmanned aerial vehicle (UAV) that could be hand-launched and would have a total mass of 10 kg. Another objective of this report is to provide an initial selection of a configuration for the solar-powered UAV. A comparative study of similar solar-powered UAVs will be discussed and will be used for a preliminary configuration for this aircraft. There will be a discussion of the propulsion system and a selection of the initial system as well as how the propulsion system will be integrated into the aircraft. Also, there will be an overall configuration that will be chosen, as well as a wing configuration and empennage configuration for the solar-powered UAV. A proposal for an initial configuration will be

shown and discussed. There will also be a weight estimate for this solar-powered UAV; an initial selection of a distribution of weights will be discussed. Since power is one of the most critical parameters for solar-powered UAVs, we will look at the fundamental equations that are important to solar-powered UAVs. Then, we will discuss their importance and how the variables in the equations will affect the design of the aircraft. Also, a stability and control analysis will be done to show how to size the empennage to account for stability. Finally, a drag polar estimation will be done using three different methods and a discussion on which method is most accurate will follow.

1.3 LITERATURE REVIEW

In this section, a brief history of solar-powered aircraft will be discussed, as well as other UAV studies that have been done over the last 20 years. Detailed mission specifications for the solar-powered UAVs that will be discussed are shown in Appendix A.

1.3.1 History of Solar-Powered Flight

To understand the history of solar-powered flight, a discussion of solar cell history is required. Humans started using the sun's rays to benefit themselves as early as 7th Century B.C., when they studied how a magnifying glass can be used to make fires. There were no major advances in solar technology until 1767 when Horace de Saussure built the world's first solar collector, later used for cooking. In 1839, Edmund Becquerel experimented with electrolytic cells and found that when these cells are exposed to light, they create electricity. This was the first ever photovoltaic cell, which is the basis of all solar cell technology. Over the next 50 years, electrolytic cells were used to power

devices, including steam engines and water heaters. Also, selenium was shown to conduct electricity when exposed to the sun. The key advancement in solar cell technology occurred in 1954 when photovoltaic technology was born in the United States. Daryl Chapin, Calvin Fuller, and Gerald Pearson created the first ever photovoltaic (PV) cell capable of using the sun's rays to power "everyday electrical equipment" [1]. Thus, PV cells were built.

On November 4, 1974, at Camp Irwin, California, the first ever solar-powered flight took place [2]. The aircraft, designed by Astro Flight Inc. and named Sunrise I, flew for 20 minutes at an altitude of 100 meters during the flight. Sunrise I was later able to fly for more than three hours, but the aircraft's career ended after it was damaged in a sandstorm. The company later built Sunrise II, which weighed less and was able to output more power in comparison to the Sunrise I.

After the Sunrise flights, there was a greater passion for solar-powered flight and many model aircraft enthusiasts began to use the solar cell technology for their aircraft. In 1996, aircraft enthusiast Dave Beck from Wisconsin built the Solar Solitude. This aircraft set model airplane records for distance flown in a straight line (38.84 km) and altitude (1283 m).

Around the same time, Wolfgang Schaeper from Germany built the Solar Excel aircraft, which was also a model aircraft. The Solar Excel broke all the model aircraft records from 1990 to 1999, including duration, distance in a straight line, gain in altitude, speed, distance in a closed circuit, and speed in a closed circuit. This aircraft still holds

all the FAI F5-SOL model aircraft records, which is astounding since it has been over a decade since Solar Excel set these records.

One example of a long endurance UAV is the SoLong aircraft. Designed by AC Propulsion, the SoLong aircraft has a wingspan of less than 5 meters and is able to fly continuously using only solar energy and thermal energy. On April 22, 2005, the SoLong aircraft flew for 24 hours and 11 minutes continuously, which was the first airplane of its kind to fly for that length of time. Two months later, the aircraft was able to fly for over 48 hours, thus opening the door for the possibility of eternal fuel-less flight.

An example of a high-altitude long endurance (HALE) UAV is the Zephyr, which was first flown in December 2005. A British company named QinetiQ first tested the Zephyr aircraft in New Mexico and it was able to fly for six hours and reach a peak altitude of 7,925 meters. The crowning achievement of the Zephyr aircraft was on September 10, 2007, when the aircraft flew continuously for 54 hours, a new world record for unmanned flight. It was able to reach a peak altitude of 17,786 meters. In the future, QinetiQ hopes to have the Zephyr aircraft do a test flight of several months at an altitude over 15,240 meters (50,000 feet).

A solar-powered manned flight was achieved with the Solar Impulse. In 2003, Bertrand Piccard started to develop a solar-powered manned aerial vehicle that will one day circumnavigate the globe using only solar power [3]. Led by Piccard, a group of engineers in Switzerland used aircraft design methodology to build a fully-functional prototype by 2009. In more recent news, the Solar Impulse completed a 26-hour flight on

July 8, 2010, using only solar energy, the first flight of its kind. They plan to complete a full circumnavigation flight in 2012.

1.3.2 Other UAV Studies

In Israel, an undergraduate student team built the SunSailor UAV to break the world record for distance flight at 139 km [4]. In 2006, successful flight tests were completed, but when the team tried for the record flight on August 12, 2006, the aircraft entered a dive and was damaged beyond repair. To this day, they are still trying to break the world record.

In 2007, NASA compared different HALE UAV concepts for a hurricane and a communications relay mission [5]. NASA separated these concepts into two categories: heavier-than-air and lighter-than-air UAVs. It was shown that no heavier-than-air concept, including the solar-powered concepts that they analyzed, could successfully complete either mission. However, the lighter-than-air concepts were able to. Despite their success, the lighter-than-air concepts had low life cycles and increased size and mass. It is important to note that NASA analyzed many different configurations of each type of propulsion concept, and provided a unique comparison of all concepts.

A study done by Tegeder [6] at Brigham Young University designed a more efficient solar-powered UAV by creating an onboard solar tracker that is programmed to move the airframe of the UAV so that the aircraft receives the most sunlight at any given time. It was found that the UAV with the solar tracker has a maximum of 34.5% gain in power output over a conventional solar-powered UAV.

In addition, a study on solar-powered, high altitude UAVs was done by Baldock [7] at Brunel University in the United Kingdom. A concept was developed to study the aerodynamics as well as the solar irradiance on the aircraft. It was shown that the HALE concept was only able to sustain year round, level flight up to latitudes of 10 degrees north, and not anywhere around the world.

1.3.3 Future Considerations

The Defense Advanced Research Projects Agency (DARPA) is currently researching a solar-powered HALE UAV. The main idea behind the new project called Vulture is to combine the key benefits of both an aircraft and a satellite into one system and to keep this system in the air continuously for five years. As of September 15, 2010, the Vulture system entered the technology phase [8], and a concept of the aircraft was designed. DARPA will continue to work with Boeing to advance this technology further and a functional prototype will be built within the next five years.

2.0 MISSION SPECIFICATION

2.1 MISSION REQUIREMENTS

2.1.1 Payload

The payload for this aircraft consists of the equipment necessary to analyze wildfires. The main components of the payload include:

- Infrared and night vision cameras, so that the aircraft can study wildfires anytime during the day or night accurately.
- Sensory equipment for wildfires.

The maximum weight of payload that will be allocated for this equipment is not to exceed 2.268 kg (5 lb).

2.1.2 Crew Members Required

This mission will require at least four crew members to fully operate the UAV. At least two crew members will need to hand-launch the aircraft, one member will pilot the UAV, and one member will be responsible for data analysis and flight tracking during the mission.

2.1.3 Range / Endurance

Range is yet to be determined in this analysis, and may not be needed because it depends on how much solar power the UAV receives and at what time the aircraft starts the mission. The maximum endurance for this aircraft will be at least ten hours at cruising altitude.

2.1.4 Cruise Speed

The maximum cruise speed for this aircraft is 30 mph, which is equivalent to around 13.5 m/s. This was chosen based on a comparison of similar aircraft.

2.1.5 Cruise Altitude

The maximum cruise altitude will be 2,000 meters. However, it is important to note that the UAV will be cruising at lower altitudes the majority of the time for data analysis.

2.1.6 Take-off and Landing

Since reduced weight is the most important consideration for a small solar-powered UAV, there will be no landing gear installed. This allows room for more solar

cells and batteries and thus more power. Therefore, the UAV will be hand-launched at take-off and will skid land softly in a designated landing area so that it does not damage the aircraft.

2.2 MISSION PROFILE

The mission profile is shown in Figure 1. Details of each phase of the mission are as follows:

- Phase 1: UAV will be hand-launched and will ideally begin to climb at 4AM continuously for 4 hours to peak cruise altitude if needed. The UAV is not required to be launched at 4AM; however, to achieve the 24-hour flight, it will need to be launched at this time.
- Phase 2: At 8AM, the UAV will cruise for a maximum of 10 hours at the peak cruise altitude of 2 km taking data.
- Phase 3: At 6PM, the UAV will begin the descent back to ground and land in the designated landing area at 4AM the next day. The UAV may not need all 8 hours to descend back to the ground, but will be designed that way to achieve the 24-hour flight.

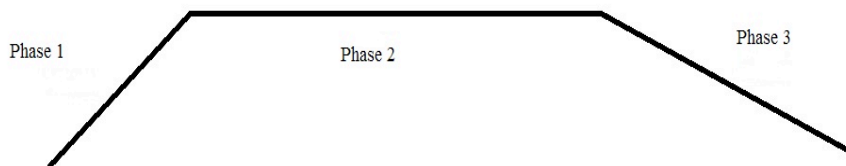


Figure 1: Solar-Powered UAV Mission Profile

2.3 MARKET ANALYSIS

The primary motivation behind building such an aircraft is the push for greener aviation. Over the last several years, many aviation companies, including NASA and Lockheed Martin, have invested in alternative fuel technology and UAVs. The Solar Impulse and the Zephyr's achievements have increased the popularity for solar-powered UAVs and MAVs, thus creating a large market for this technology. There has also been a need for studying disasters such as wildfires and the Gulf oil spill in a safe, efficient way. Many firefighters risk their lives putting out fires and a small UAV, such as the solar-powered aircraft discussed in this report, would be an asset to them.

2.4 TECHNICAL AND ECONOMIC FEASIBILITY

Although solar-powered UAVs are more expensive to build because of the advanced technology used, they would be more fuel efficient and would require less maintenance compared to a fueled UAV. Since the solar-powered UAV will not require any jet fuel, it can save millions of dollars over a long period of time and help save the environment.

During the design and developing phases, it will take an engineering crew of over 10 members to build this aircraft. If there is a need for mass production, more crew members will be required. Building the aircraft will be relatively simple since most of the products can be mass produced fairly easily, and equipment such as solar cells, batteries, and cameras is readily available.

2.5 CRITICAL MISSION REQUIREMENTS

The critical mission requirements that will drive the design of this aircraft are as follows:

- Total mass must be less than 10 kg
- Total endurance will be no less than 24 hours
- Must be capable of carrying a payload no more than 2.27 kg (5 lbs)

3.0 COMPARATIVE STUDY OF SIMILAR AIRPLANES

In this section the airplanes that will be studied are the Sunrise I and II, Solar Solitude, Solar Excel, SoLong, Zephyr, and the SunSailor 1 and 2.

3.1 MISSION CAPABILITIES AND CONFIGURATION SLECTION

The mission capabilities and configuration selection for the studied aircraft are shown in Tables 1 and 2. As you can see, most of the capabilities of these aircraft are minimal and used primarily to study the potential of solar-powered long-endurance flight. Most of the aircraft have a single propeller conventional configuration with a v-tail.

Table 1: Mission Capabilities for Sunrise I and II, Solar Solitude, and Solar Excel

	Sunrise I	Sunrise II	Solar Solitude	Solar Excel
Capabilities	1 st ever solar-powered flight. Minimal capabilities.	Improved on Sunrise I on power output and weight. Minimal capabilities.	Model aircraft, minimal capabilities. Set records for distance and altitude in FAI F5-SOL category in Aug. 1996.	Minimal capabilities. Holds all records in FAI F5-SOL category.
Configuration	Single propeller conventional configuration with conventional tail.	Same as Sunrise I.	Single propeller conventional configuration with t-tail.	Single propeller conventional configuration with v-tail.
Solar Cell Configuration	4096 solar cells.	4480 solar cells at 14% efficiency.	Unknown.	Unknown.
Power Output	450 W.	600 W.	Unknown.	Unknown.

Table 2: Mission Capabilities for SoLong, Zephyr, and SunSailor 1 and 2

	SoLong	Zephyr	SunSailor 1	SunSailor 2
Capabilities	Minimal capabilities. Flew continuously for 48 hours using solar cells and electric motor.	Used by military for reconnaissance and communications platforms. Civilian programs will use it for ground observation.	Minimal capabilities. Used to break range world record for F5-SOL category (still has not been broken).	Same as SunSailor 1.
Configuration	Single propeller conventional configuration with v-tail.	Two propeller conventional configuration with t-tail.	Single propeller conventional configuration with v-tail.	Same as SunSailor 1.
Solar Cell Configuration	120 Sanyo 1850 Li-Ion cells, 76 Sunpower A300 solar cells, nominal power = 225 W, battery mass = 5.50 kg.	Batteries are Lithium Sulfur batteries from Sion.	Sunpower A300 solar cells with 21% efficiency, 0.943 m ² area, weighs 0.66 kg total.	Sunpower A300 solar cells with 21% efficiency, 1.097 m ² area, weighs 0.77 kg total.
Power Output	Maximum motor power: 800 W.	Unknown.	PV's max power is 100 W.	PV's max power is 140 W.

3.2 COMPARISON OF IMPORTANT DESIGN PARAMETERS

The important design parameters are shown in Table 3. The complete list of design parameters for the aircrafts that were studied can be found in Appendix A. If the Zephyr aircraft is excluded, the total weight of each aircraft does not exceed 13 kg. No aircraft exceed 10 meters in wingspan length except the Zephyr, and their aspect ratios range between 11.4 and 13.3. Therefore, to build a successful solar-powered aircraft, a low weight design with a high aspect ratio and relatively high wingspan is necessary.

Table 3: Important Design Parameters for Similar Aircraft

	Sunrise I	Sunrise II	Solar Solitude	Solar Excel	SoLong	Zephyr	SunSailor 1/2
Weight (in kg)	12.25	10.21	2	0.72	12.6	50	3.6
Endurance	Maximum flight time was 4 hours	Unknown	Unknown	11 hours, 34 minutes, 18 seconds	48 hours, 16 minutes	336 hours, 21 minutes (Over 14 days)	Unknown
Wingspan (in m)	9.75	9.75	2.7	2.1	4.75	22.5	4.2
Aspect Ratio	11.4	11.4	13.3	12.8	15	11.6	13.15

4.0 COMPARATIVE STUDY OF AIRPLANES WITH SIMILAR MISSION PERFORMANCE

The configurations and capabilities of similar aircraft are shown in Tables 1 and 2 (See Section 3.1). These aircraft consist of a single engine propeller propulsion system. This was chosen because current technology allows propellers to be powered by electric motors, which require no gas and are required for solar-powered aircraft. The high wing configuration is chosen because of no landing gear and weight savings. The wing needs to be as far away from the ground as possible to reduce damage. Since the wing has photovoltaic cells and sometimes batteries, it becomes the most expensive part of the aircraft; thus, avoiding damage to the wing is a priority.

For the empennage, there are three options that are most common to solar-powered aircraft: v-tail, t-tail, and conventional. The v-tail configuration provides better stability than the other configurations, and also reduces weight. The t-tail configuration is optimum for integrating solar cells onto the tail to increase power, but there is a significant weight increase in comparison to the v-tail. A conventional tail is used in most aircraft, but it is rarely used for a solar-powered aircraft because if there were solar cells on the horizontal stabilizer, half of them could be unused due to the vertical stabilizer producing shade on one side. A conventional configuration also adds weight to the aircraft, which is critical for solar-powered UAVs.

5.0 SELECTION OF PROPULSION SYSTEM

5.1 SELECTION OF THE PROPULSION SYSTEM TYPE

The propulsion system type will be electrical with photovoltaic cells powering the motors and payload.

5.2 SELECTION OF THE NUMBER OF ENGINES

There will be a single engine propeller located at the tip of the fuselage, just ahead of the wing. Many small solar-powered aircraft are equipped with a single engine propeller because the aircraft is light enough to be powered by only one propeller. The thrust-to-weight ratio is a critical parameter for the selection of engines, and since smaller solar-powered aircraft are very light, they need a minimal amount of thrust to takeoff. Larger aircraft, such as the Solar Impulse and AeroVironment's Helios, need multiple engines because of the size and weight.

5.3 PROPELLER SIZING

Depending on how large the diameter of the fuselage is, the propeller sizing can vary. The larger the propeller diameter, the more efficient the propeller becomes. One of the limitations that Raymer [9] discusses is the propeller tip speed, which is the sum of the rotational speed and the aircraft's forward speed, as shown in (3.1) and (3.2).

$$(V_{tip})_{static} = \pi n d / 60 \quad (3.1)$$

$$(V_{tip})_{helical} = \sqrt{V_{tip}^2 + V^2} \quad (3.2)$$

To determine the propeller diameter, Roskam [10] uses data from other aircraft and (3.3) to determine the ideal propeller diameter based on the maximum power per engine, number of propeller blades, and the power loading per blade.

$$D_p = \left(\frac{4P_{\max}}{\pi n_p P_{bl}} \right)^{1/2} \quad (3.3)$$

A propeller that is readily available would be ideal for a small solar-powered aircraft because it can be purchased and installed easier. For an initial selection, a propeller with an 11 inch diameter with a 6-8 inch pitch and a rotational speed of 1000-2000 rpm will be selected. To keep the efficiency the highest, it is necessary to use a gearbox to connect the propeller and motor together.

6.0 CONFIGURATION SELECTION

6.1 OVERALL CONFIGURATION

Based on Roskam, a land-based conventional configuration is used for the solar-powered UAV. The solar-powered UAV will be controlled by a pilot on land and thus will primarily fly on land and not water. Adding a hybrid system would only add weight, which is not recommended.

6.2 WING CONFIGURATION

The wing selection is a vital part for a solar-powered aircraft because not only should the wing have good aerodynamic characteristics, but it also must be suitable for solar cells to be added onto the top surface of the wing. For this solar-powered aircraft, a

high cantilever wing will be selected primarily for simplicity and to provide enough clearance for a skid landing. A high wing also provides better lateral stability, which is needed since there will be minimal stabilizing devices on this type of aircraft.

The geometry of the wing should have negligible sweep because the aircraft will be operating at low speeds. Sweep will also increase weight and reduce the available solar cell area, both of which will hinder the aircraft's performance. An initial airfoil selection will be the Selig 1223, as shown in Figure 2. This airfoil has a 12.14% maximum thickness-to-chord ratio at roughly 20% from the leading edge.

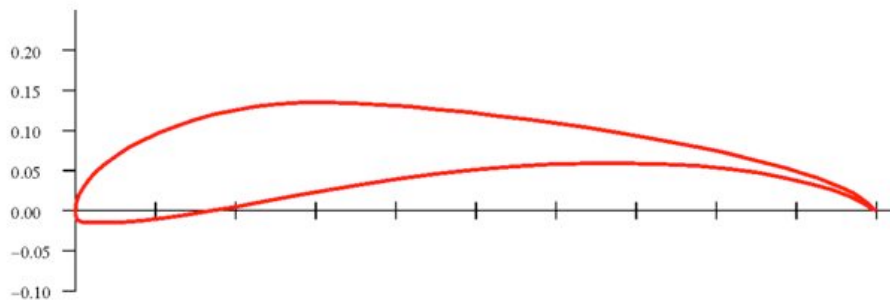


Figure 2: Selig 1223 Airfoil with Unit Chord Length

The Selig 1223 airfoil was chosen as the initial configuration because it has good aerodynamic characteristics that are important for a solar-powered UAV. The primary important characteristic of this airfoil is that it is a low Reynolds number airfoil. Since this solar-powered aircraft will be flying at low speeds, a low Reynolds number will be generated throughout the mission, and therefore an airfoil that has ideal characteristics at low speeds has been chosen. Another main characteristic of this airfoil is a high lift-to-drag ratio. Using XFLR5 software that analyzes airfoils, a graph of L/D vs. angle of attack was created and is shown in Figure 4. A legend that is used for the different

Reynolds numbers used is shown in Figure 3. As the figures show, not only does this airfoil have a high lift-to-drag ratio, but it also has a fairly wide operating angle of attack where the lift-to-drag ratio is optimum. Other airfoil characteristics are shown in Figures 5, 6, and 7.

The aircraft will have no geometric or aerodynamic twist because it needs to absorb as much solar energy as possible, and the optimum geometry to do that would require no wing twist. There is a possibility that the aircraft will have a slight dihedral angle and winglets in the final configuration; however it has not been determined if these are needed. This aircraft will also have no high lift devices because that would add weight.

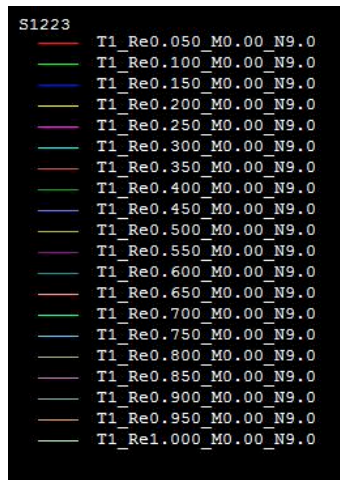


Figure 3: XFLR5 Reynolds Number Legend (0.050 is 50000, 0.1 is 100,000, etc.)

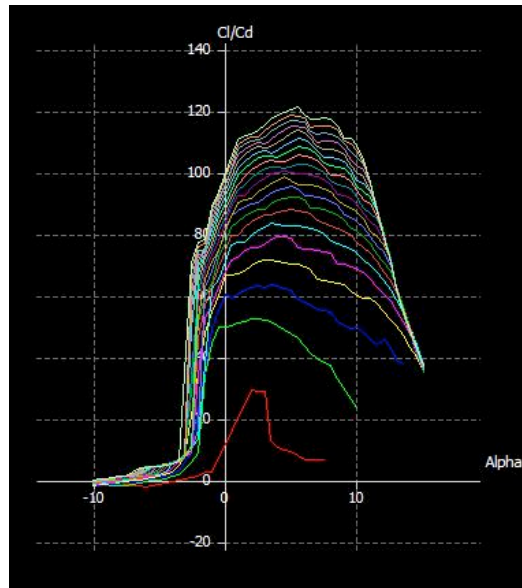


Figure 4: Lift-to-Drag Ratio as a Function of Angle of Attack for Selig 1223 Airfoil

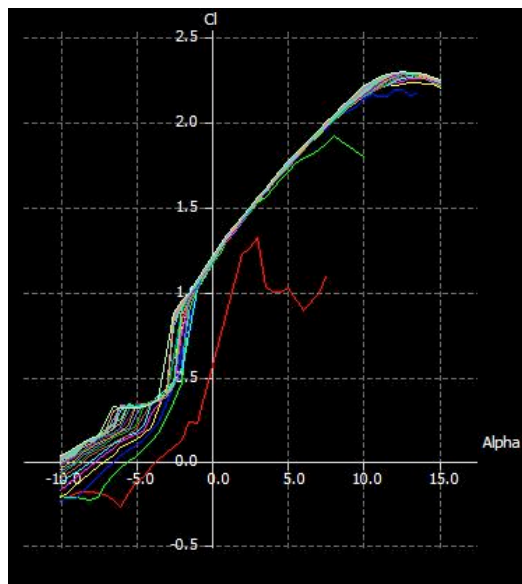


Figure 5: Lift Coefficient as a Function of Angle of Attack for Selig 1223 Airfoil

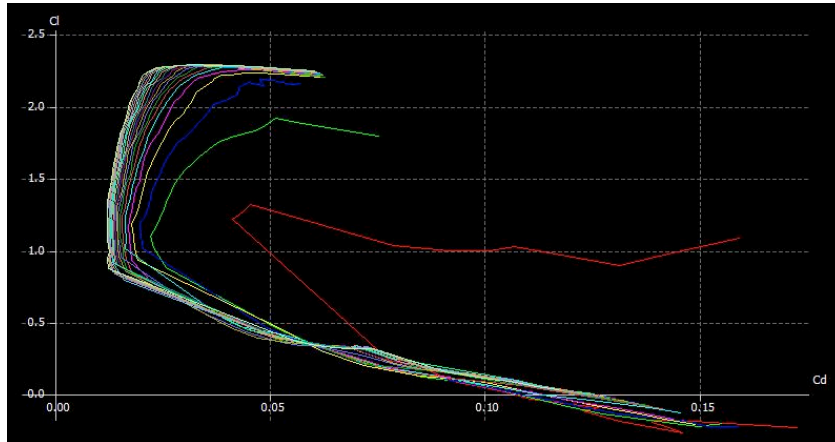


Figure 6: Lift Coefficient as a Function of Drag Coefficient for Selig 1223 Airfoil

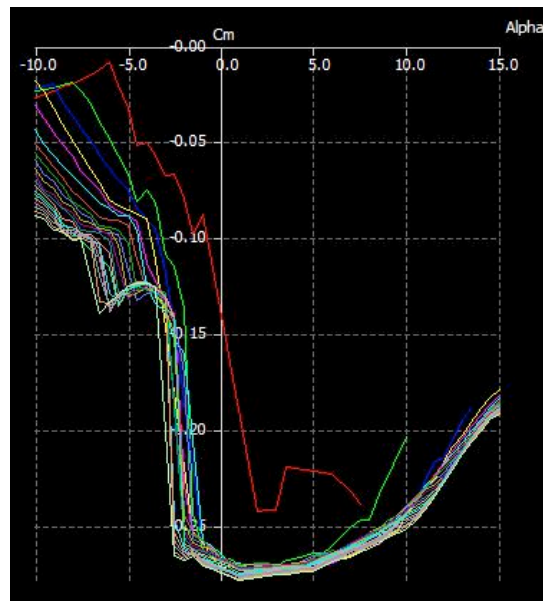


Figure 7: Moment Coefficient as a Function of Angle of Attack for Selig 1223 Airfoil

6.3 EMPENNAGE CONFIGURATION

The solar-powered UAV will incorporate a v-tail empennage configuration because of weight savings and stability. Another configuration that will be considered is the conventional configuration because it will be easier to build.

6.4 LANDING GEAR DISPOSITION

This solar-powered aircraft will not have any landing gear installed. Instead, it will be designed to skid land in a designated landing area. The main consideration for a skid landing will be the size of the fuselage. The fuselage will need to be large enough so that it clears the propeller distance, but small enough so that it does not increase the overall drag of the aircraft.

6.5 PROPOSED CONFIGURATION

One proposed configuration is shown in Figure 8. For simplicity, a cylindrical fuselage is chosen for an initial configuration. Over time, the exact shape of the fuselage will be better defined. The v-tail empennage, as well as the high wing configuration, will be the same for all configurations. For the configuration shown, there is a straight fixed wing with dihedral midway on each side of the wing. Another configuration that will be considered will be a straight fixed wing with no dihedral. Finally, there will be a configuration that will use both dihedral and winglets. Other views of the initial configuration are shown in Appendix B.

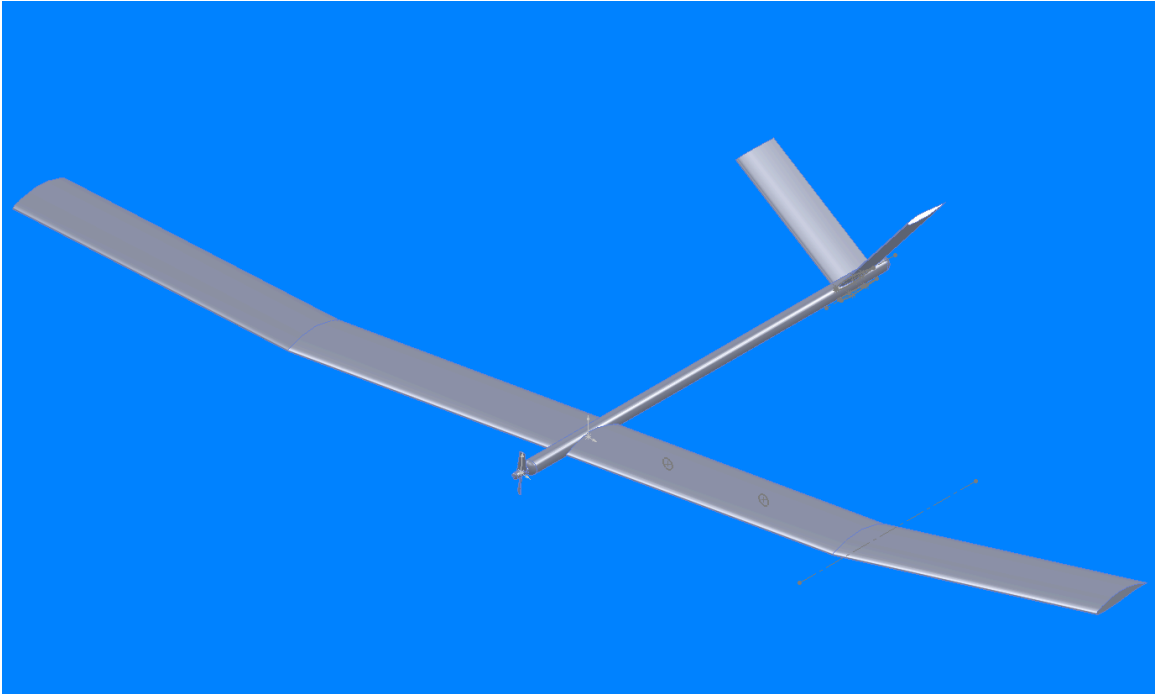


Figure 8: Solar-Powered UAV Proposed Configuration

7.0 MISSION WEIGHT ESTIMATES

7.1 COMMENTS

Before the calculation of weights is determined, a few factors should be considered. First, the weight of solar-powered aircraft differs from the weight of other aircraft because there is no fuel weight. In most commercial aircraft, fuel weight is an important variable when calculating the takeoff weight versus the empty weight of the aircraft. Since the solar-powered aircraft runs on photovoltaic cells, there is no empty weight or fuel weight distinction. Therefore, a weight analysis cannot be done by using the steps in Roskam and Raymer. However, Noth [11] goes into detail about weight prediction models and how it is possible to obtain an appropriate estimate of the

component weight simply by inserting the relative parameters that pertain to the aircraft. Therefore, Noth's method of determining weights will be used since the method is more applicable to this research.

7.2 DATABASE FOR WEIGHTS OF SIMILAR AIRCRAFT

Noth provides a graph of weight as a function of wing loading for unmanned and manned solar powered aircraft. The total mass, aspect ratio, and wing area for the proposed design are shown below in Table 4. Calculations for the total mass are shown in Section 7.3. The proposed design is most comparable to the Sunrise I and II aircraft.

Table 4: Mission Parameters and Calculation of Weight and Wing Loading

Total Mass	9.65 kg
Wingspan	7 m
Aspect Ratio	13
Wing Area	3.77 m ²
Weight = $W = mg$	94.67 N
Wing Loading = W/S	25.11 N/m ²

7.3 DETERMINATION OF MISSION WEIGHTS

The following sections provide information regarding the calculation of most of the component weights. All equations from each section are from Noth [11] and are used only as initial estimates of the various weights. The variables for each of these equations can be found in Appendix C.1, where the initial parameters are given. The definition of each symbol that appears in this section is listed in the List of Symbols section.

7.3.1 Determination of Power Available

For this aircraft, it is assumed that it is at steady level flight. Thus, the thrust that the aircraft generates will be equal to the total drag force. Also, the total lift force will equal the total weight. This is shown in (7.1) and (7.2):

$$mg = C_L \frac{\rho}{2} SV^2 \quad (7.1)$$

$$T = C_D \frac{\rho}{2} SV^2 \quad (7.2)$$

After solving for velocity in (7.1), then taking into consideration that the power required for steady level flight is thrust multiplied by velocity, then (7.3) can be used to calculate the power required for steady level flight:

$$P_{lev} = Tv = \frac{C_D}{C_L^{3/2}} \sqrt{\frac{2ARg^3}{\rho}} \frac{m^{3/2}}{b} \quad (7.3)$$

To calculate the daily required electrical energy that the aircraft must use for steady level flight, (7.4) is used:

$$P_{electot} = \frac{1}{\eta_{ctrl}\eta_{mot}\eta_{grb}\eta_{plr}} P_{lev} + \frac{1}{\eta_{bec}} (P_{av} + P_{pld}) \quad (7.4)$$

Equations (7.1) through (7.4) will be used for the weight analysis of some components for the solar-powered aircraft.

7.3.2 Fixed Masses

Following Noth's mass prediction models, the fixed mass can be defined using (7.5):

$$m_{fixed} = m_{av} + m_{pld} \quad (7.5)$$

For the initial calculations, 2.27 kg (5 lb) was chosen as the mass of the payload and 1 kg as the mass of the avionics.

7.3.3 Mass of Airframe

Noth uses a statistical analysis to show how the airframe mass depends on the aspect ratio and wingspan of the aircraft. He then chooses constants that go into (7.6):

$$m_{af} = k_{af} AR^{x_2} b^{x_1} \quad (7.6)$$

The constants x_1 and x_2 will remain the same as in Noth's models, but for k_{af} , a constant that is 20% the value of Noth's will be used for this aircraft.

7.3.4 Mass of Solar Cells

To come up with an accurate mass of the amount of solar cells on the aircraft, the solar cell area must be defined. Noth provides an equation, shown in (7.7), that relate the solar cell area to efficiency variables, maximum irradiance, and the time of day and night, as well as the total electric power available:

$$A_{sc} = \frac{\pi}{2\eta_{sc}\eta_{cbr}\eta_{mpp}\eta_{max}\eta_{wthr}} \left(1 + \frac{T_{night}}{T_{day}} \frac{1}{\eta_{chrg}\eta_{dchrg}} \right) P_{electot} \quad (7.7)$$

For the proposed design, 1040 W/m^2 was chosen as the maximum radiance, which is the irradiance found at 37 degrees north latitude on June 23 [12]. This latitude is for San Jose, CA, where the solar-powered aircraft will take off from. Using (7.7) the total solar cell mass can be defined using (7.8):

$$m_{sc} = A_{sc}(k_{sc} + k_{enc}) \quad (7.8)$$

Equation (7.8) accounts for the need of encapsulating the solar cells so that they are not damaged in flight.

7.3.5 Mass of Maximum Power Point Tracker

The maximum power point tracker is a device that provides the highest amount of energy to the batteries. This device tracks the peak value of the energy that is absorbed by the solar cells, and then transfers that amount to the batteries for storage and to propel the aircraft. The mass of the maximum power point tracker can be found using (7.9):

$$m_{mppt} = k_{mppt} I_{\max} \eta_{sc} \eta_{cbr} \eta_{mppt} A_{sc} \quad (7.9)$$

7.3.6 Mass of Batteries

Although batteries are an essential part of a solar-powered aircraft because they provide the power for overnight flying, they also add a significant amount of weight to the aircraft. Equation (7.10) is used to find the total amount of allowable mass for batteries:

$$m_{bat} = \frac{T_{night}}{\eta_{dchrg} k_{bat}} P_{electot} \quad (7.10)$$

7.3.7 Mass of Propulsion Group

The propulsion group will consist of the following components: the electric motors, control electronics, gearboxes, and propellers. Using the statistical analysis from Noth, the mass of the entire propulsion group can be calculated using (7.11):

$$m_{prop} = k_{prop} P_{lev} \quad (7.11)$$

7.3.8 Results

The above subsections are used to calculate the various masses of the entire solar-powered aircraft. Using Matlab, these equations are optimized for a certain wingspan and total mass, and the m-files are shown in Appendix B. The parameters are also shown in Appendix C under InitParameters2.m. Figures 9 and 10 show the results of this analysis. We see that for a total mass of 10 kg, a wingspan of 7 m will be needed. The breakdown of the mass distribution is shown in Table 5.

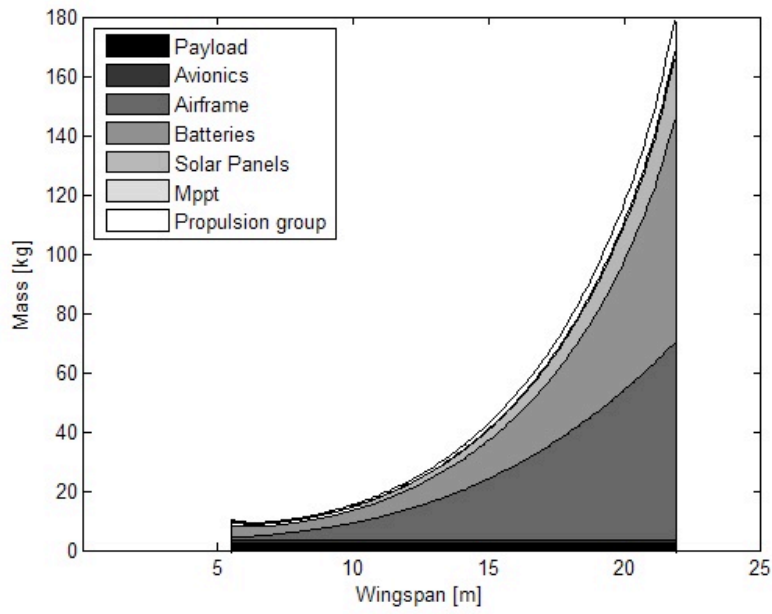


Figure 9: Wingspan versus Mass Distribution

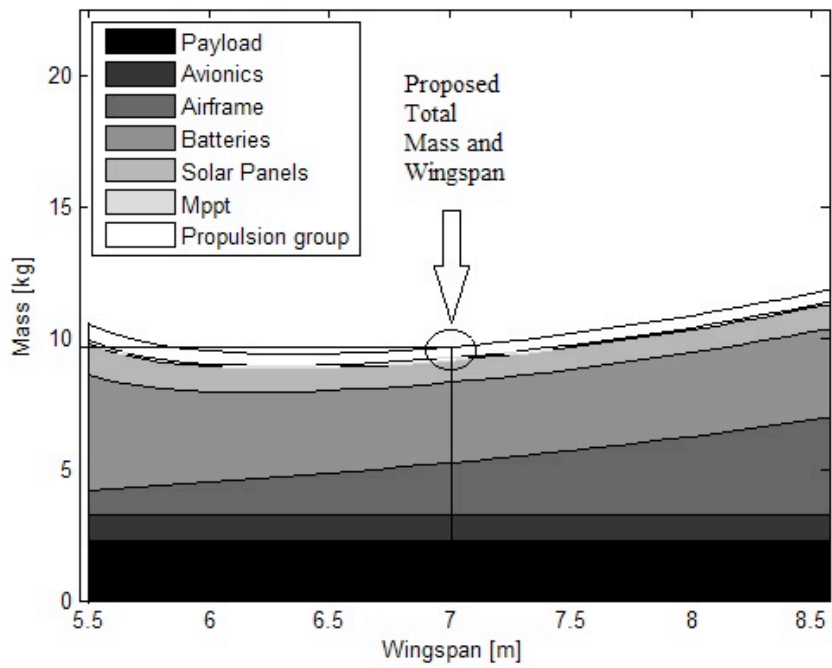


Figure 10: Proposed Mass and Wingspan

Table 5: Breakdown of Mass Available for Components

Components	Mass (in kg)
Payload	2.268
Avionics	1
Airframe	1.962
Batteries	3.06
Solar Panels	0.84
Maximum Power Point Tracker (MPPT)	0.1
Propulsion Group	0.42
TOTAL	9.65

8.0 PERFORMANCE CONSTRAINT ANALYSIS

8.1 COMMENTS

From our weight estimate analysis, we have defined a wingspan, wing area, and aspect ratio. Since these are only estimates, these values cannot be used until a performance constraint analysis is completed. The parameters shown in Table 6 will be the parameters that this aircraft will need to meet during the mission.

Table 6: Critical Mission Parameters

Aspect Ratio	13
Maximum Cruise Velocity	13.5 m/s (30 mph)
Weight	98.1 N (22 lbs)
Cruise Altitude	2,000 m
Rate of climb	1 ft/s (0.3 m/s)

8.2 SIZING TO CRUISE SPEED REQUIREMENTS

To calculate the cruise speed requirement, Roskam uses a Power Index formula which is shown in (8.1):

$$I_p = \left[\frac{\left(\frac{W}{S} \right)}{\sigma \left(\frac{W}{P} \right)} \right]^{1/3} \quad (8.1)$$

Roskam provides a graph of how aircraft speed and the Power Index variable are related, which is shown in Figure 11. In Figure 11, a maximum cruise speed of 30 mph will result in a power index of 0.1714. This value is inserted into (8.1) to determine the relationship between the wing loading (W/S) and power loading (W/P). For (8.1), the air density ratio is defined at 2,000 m and is 0.82168.

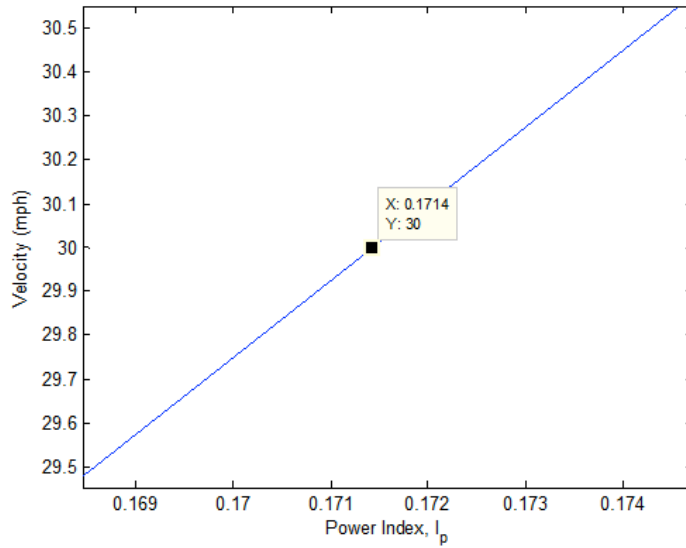


Figure 11: Correlation between Aircraft Speed and Power Index

8.3 SIZING TO FAR 23 RATE OF CLIMB REQUIREMENTS

In Table 6, the rate of climb requirement was set at 0.3 m/s. This is quite ambitious for a solar-powered aircraft; however, it is much lower than a conventional aircraft's climb requirement. Roskam defines the rate of climb in (8.2):

$$RC = \frac{dh}{dt} = 33,000(RCP) \quad (8.2)$$

The rate of climb parameter is also defined by Roskam in (8.3):

$$RCP = \frac{\eta_{plr}}{\frac{W}{P}} - \frac{\left(\frac{W}{S}\right)^{1/2}}{19 \left(\frac{C_L^{3/2}}{C_D}\right) \sigma^{1/2}} \quad (8.3)$$

A propeller efficiency of 50%, an air density ratio at 2,000 m of 0.82168, a lift coefficient of 1.5, and a drag coefficient of 0.0967 is assumed. The drag coefficient was solved for using (8.4) below:

$$C_D = C_{D_{aft}} + C_{D_{par}} + C_{D_0} = C_{D_{aft}} + C_{D_{par}} + \frac{C_L^2}{\pi e AR} \quad (8.4)$$

Assuming an Oswald efficiency factor of 0.9, and using the initial parameters that were in Noth's model (See Appendix C.1), the total drag coefficient was calculated. A relationship between our wing loading and power loading to meet our climb requirements can now be determined.

8.4 PERFORMANCE SIZING GRAPH

Using the two correlations defined in Section 8.2 and 8.3, the wing loading versus power loading relationships can be determined and are shown in Figure 12. In Figure 12, the three curves represent the various requirements: cruise speed, rate of climb, and takeoff speed. Roskam uses a value of 70% of the cruise speed requirement. The intersection point between the curves is the optimum design point and will help determine the power required and wing area required for the mission. Since the graph has two intersection points, the point that uses the takeoff and the rate of climb requirements is chosen because if the takeoff requirement is met, then the cruise requirement will also be met. The coordinates of this point are (W/S, W/P) = (0.9715, 0.2204).

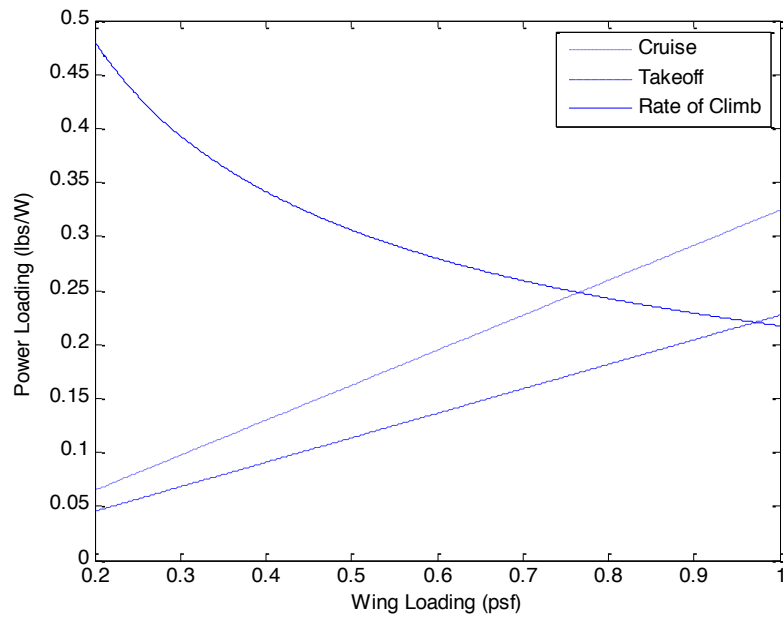


Figure 12: Performance Sizing Graph

Using the wing loading and power loading values, the power required and the wing area for the aircraft can be determined:

$$\frac{W}{P} = 0.2204 \rightarrow P = \frac{W}{0.2204} = \frac{(10\text{kg})(9.81\text{m/s}^2)(0.2248\text{lb/N})}{0.2204} = 100.06W$$

$$\frac{W}{S} = 0.9715 \rightarrow S = \frac{W}{0.9715} = \frac{(10\text{kg})(9.81\text{m/s}^2)(0.2248\text{lb/N})}{0.9715} = 22.7\text{ft}^2 = 2.11\text{m}^2$$

Using the given aspect ratio of 13, the new wingspan can be solved for:

$$AR = \frac{b^2}{S} \rightarrow b = \sqrt{(AR)(S)} = \sqrt{(13)(2.11\text{m}^2)} = 5.24\text{m}$$

The new wing chord length can now be calculated:

$$S = bc \rightarrow c = \frac{S}{b} = \frac{2.11m^2}{5.24m} = 0.403m$$

8.5 POWER ANALYSIS

The power available from Section 8.4 was determined to be approximately 100 W. This does not take into account the efficiencies of the propeller or motor that will be used. As an initial estimate, the propeller efficiency and motor efficiency will be 50% and 85% respectively. Thus, the total amount of power required can be solved for:

$$P = \frac{100.06W}{(0.5)(0.85)} = 235.4W$$

The solar cell type must be known before the power outputted by the solar panels is calculated. For this aircraft, the AzurSpace's S 32 solar cell will be used for its low weight and high efficiency. Noth used a configuration of 36 solar cells connected twice in series, and it was found that the total power output was approximately 30 W. Using this configuration, the power output per solar cell is approximately 0.42 watts per solar cell. Knowing the dimensions of the solar cell to be 31.9 mm by 74 mm, the maximum number of solar cells that can be installed onto the wing can be calculated:

$$c = 0.403m \rightarrow y = \frac{0.403m}{0.0319m} = 12$$

$$b = 5.24m \rightarrow x = \frac{5.24m}{0.074m} = 70$$

Thus, the total number of solar cells that can be installed on the wing is 840. The power outputted by the solar cells can now be calculated:

$$P = (840_{sc})(0.42W / sc) = 350W$$

From this analysis, it is clear that this aircraft will have enough available solar cell power to complete its mission. This is not taking into account the camber of the airfoil, as well as weather conditions. The assumption that the entire wing is covered with solar cells is also not valid since there will be control surfaces on the trailing edge of the wing that cannot have solar panels installed on them.

8.5 STALL SPEED

Roskam provides an equation for stall speed for steady level flight which is shown in (8.5):

$$V_{stall} = \sqrt{\frac{2W}{\rho S C_{L_{max}}}} \quad (8.5)$$

It is known that the cruising altitude will be 2,000 m, which corresponds to a density of 1.0066 kg/m³. Other variables that are needed include the wing area, maximum lift coefficient, and the total mass of the aircraft. It was previously shown that these values are 2.11 m², 1.5, and 10 kg, respectively. Therefore, the stall speed can now be determined:

$$V_{stall} = \sqrt{\frac{2W}{\rho S C_{L_{max}}}} = \sqrt{\frac{2(10kg)(9.81m / s^2)}{(1.0066kg / m^3)(2.11m^2)(1.5)}} = 7.85m / s$$

9.0 FUSELAGE DESIGN

The fuselage design for a solar-powered aircraft is relatively simple since there is no fuel needed or passengers to load onto the aircraft. The primary components that will go into the fuselage will be the payload, autopilot computer, batteries, and a motor for the propeller. To size the fuselage, a comparison of similar aircraft was used. For this analysis, the SunSailor [4] and Sky-Sailor [11] designs were most applicable. A comparison of the fuselage length versus wingspan was done for these two aircraft and the relationship that was found is shown in (9.1):

$$F_L = b^{0.5289} \quad (9.1)$$

Using the wingspan that was calculated in Section 8.4, the fuselage length for the aircraft is 2.4 m.

There will be two primary sections of the fuselage design. One section will include the payload, electronic, and propulsion equipment. This section will be cylindrical in shape for ease of building. This section will stretch from the tip of the fuselage to the midpoint of the fuselage length, which is 1.2 m. The diameter of this section was chosen from Raymer to have a maximum of 0.4 m to minimize subsonic drag. The other section of the fuselage will be made from a smaller diameter aluminum tube for simplicity and weight savings. The diameter for this section will be 1 inch. Please refer to Appendix D for a CAD drawing of the fuselage using the dimensions specified.

10.0 WING, HIGH LIFT SYSTEM, AND LATERAL CONTROLS DESIGN

10.1 WING PLANFORM DESIGN

From the power analysis, the gross wing area was determined to be 2.11 m^2 , and the aspect ratio was determined to be 13. Throughout this section, the taper ratio, dihedral angle, sweep angle, and twist angle for our wing will be defined and calculated. Also, any high-lift devices or control surfaces that will be used on the wing will be discussed.

10.2 TAPER RATIO

Taper ratio is defined as the ratio of the wing tip chord to the wing root chord. Raymer indicates that for a rectangular unswept wing, the taper ratio should be close to 0.45 in order to have an elliptical lift distribution throughout on the wing. For this aircraft, the taper ratio will be 1, meaning that there will be no change in wing chord from tip to root. The main reason why this was chosen is because there needs to be enough area to install the solar panels onto so that there is enough power to fly.

10.3 DIHEDRAL ANGLE

Dihedral angle on the wing is primarily used for increasing the dihedral effect of the aircraft. The dihedral effect is a rolling moment that results from the aircraft having a non-zero sideslip angle. Thus, the dihedral is primarily used to stabilize the aircraft. For this aircraft, a dihedral will be added in towards the root 0.5 m from the tip on each side of the wing. This dihedral was chosen because it is where the ailerons will be installed. The majority of the wing will also be parallel to the ground, thus generating the most lift. A 6° angle will be chosen based on a comparison of similar aircraft.

10.4 INCIDENCE ANGLE

The incidence angle of the aircraft is the angle between the chord line of the wing and the longitudinal axis of the fuselage. This value is fixed because it depends on how the wing is mounted onto the fuselage. Looking at similar aircraft, zero or very little angle of incidence is used. Therefore for this aircraft, there will be no incidence angle applied.

10.5 AIRFOIL SELECTION

The wing airfoil that was chosen will be the Selig 1223, as was discussed in Section 6.2.

10.6 HIGH LIFT DEVICES

High lift devices are primarily used for takeoff and landing to control the aircraft and provide extra lift during climb. For this aircraft, there will be no high lift devices installed because they add to the overall weight of the aircraft.

10.7 CONTROL SURFACES

The control surfaces that will be installed on the wing will be ailerons, which are devices on the trailing edge that help maneuver and control the aircraft. Raymer suggests using ailerons that extend from 50% to 90% on each side of the wing. Therefore, the ratio between the total aileron span and the wing span will be 0.4. Raymer also suggests that for the span ratio of 0.4, the chord ratio should be between 0.2 - 0.24. Based on this analysis, 22% of the total wing chord length will be used for the aileron chord length. The total aileron surface area, span length, and chord length for this aircraft are shown in Table 7.

Table 7: Aileron Dimensions

Aileron Span	2.096 m
Aileron Chord	0.08866 m
Total Aileron Surface Area	0.1858 m ²

10.8 WING CAD DRAWING

The complete wing CAD drawing was done using XFLR5 and the views are shown in Appendix E.

11.0 EMPENNAGE DESIGN AND CONTROLS ANALYSIS

11.1 OVERALL EMPENNAGE DESIGN

In Section 6.3 it was determined that this aircraft will incorporate a v-tail empennage. This section will specify the dimensions of the empennage in more detail.

The location of the empennage will be calculated using Raymer's methods for a front-mounted propeller engine. Raymer suggests that the tail arm should be 60% of the fuselage length. The tail arm is defined as the distance from the tail quarter-chord to the wing quarter-chord. Using the fuselage length of 2.4 m, the tail arm can be solved for:

$$L_{VT} = L_{HT} = 0.6(2.4m) = 1.44m$$

To calculate the tail area, the total horizontal and vertical areas are calculated using (11.1) and (11.2) below:

$$S_{VT} = \frac{c_{VT}bS}{L_{VT}} \quad (11.1)$$

$$S_{HT} = \frac{c_{HT}cS}{L_{HT}} \quad (11.2)$$

The values for the horizontal and vertical tail volume coefficients will be used from Roskam for sailplanes. Using these values, as well as the values that were calculated so far for the aircraft, the horizontal and vertical area can be determined:

$$S_{VT} = \frac{c_{VT}bS}{L_{VT}} = \frac{(0.02)(5.24)(2.11)}{(1.44)} = 0.15356m^2$$

$$S_{HT} = \frac{c_{HT}cS}{L_{HT}} = \frac{(0.5)(0.403)(2.11)}{(1.44)} = 0.2953m^2$$

The v-tail will now need to be sized accordingly so that it has the same total surface area.

To do this, the tail dihedral angle will be determined using Raymer's methods:

$$\alpha_{TD} = \arctan\left(\sqrt{\frac{S_{VT}}{S_{HT}}}\right) = \arctan\left(\sqrt{\frac{0.15356}{0.2953}}\right) = 35.8^\circ$$

Using this angle, as well as the horizontal area calculated above, the total area for one side of the v-tail can be calculated:

$$S_T = \frac{S_{HT}/2}{\cos(\alpha_{TD})} = \frac{0.2953/2}{\cos(35.8^\circ)} = 0.182m^2$$

After a comparison of similar aircraft, the tail chord length can be assumed to be 60% of the wing chord length. Using this assumption, the tail chord length is calculated to be 0.2418 m. Using the tail dihedral angle, the actual total wingspan of the entire v-tail is 1.856 m. Using this value, and knowing that the chord length is 0.2418 m, it can be calculated that the aspect ratio of the v-tail is 7.68.

11.2 EMPENNAGE AIRFOIL

For the v-tail empennage, a comparison of similar aircraft suggests that a NACA 0008 airfoil be used for simplicity and controllability. An analysis was done using XFLR5 of the NACA 0008 airfoil, and the results are shown in Figures 13 through 17.

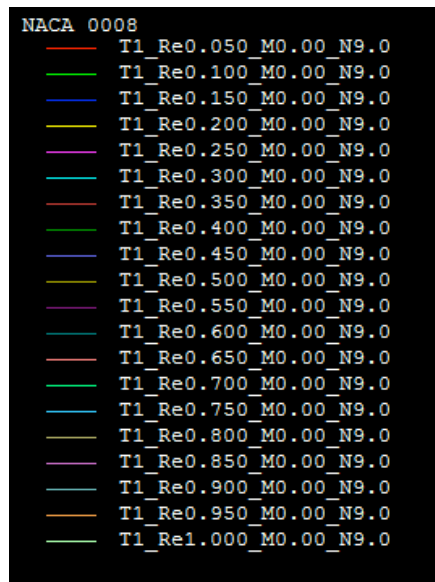


Figure 13: NACA 0008 Reynolds Number Legend

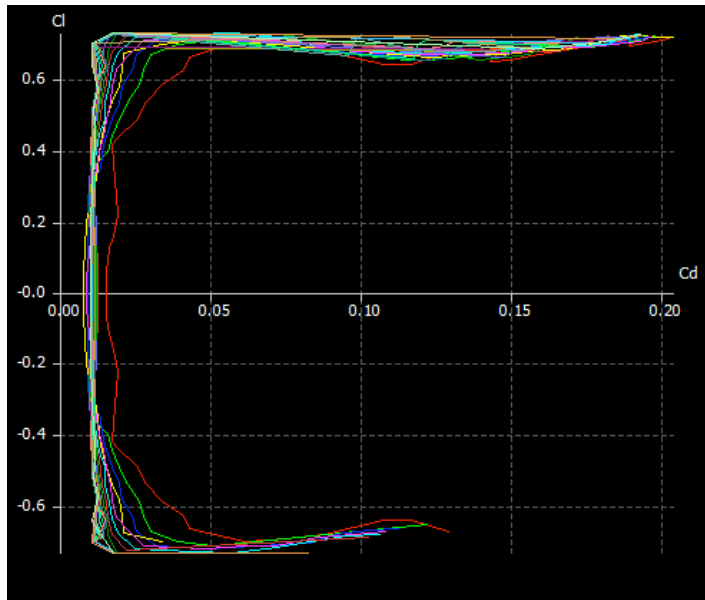


Figure 14: Lift Coefficient versus Drag Coefficient for NACA 0008

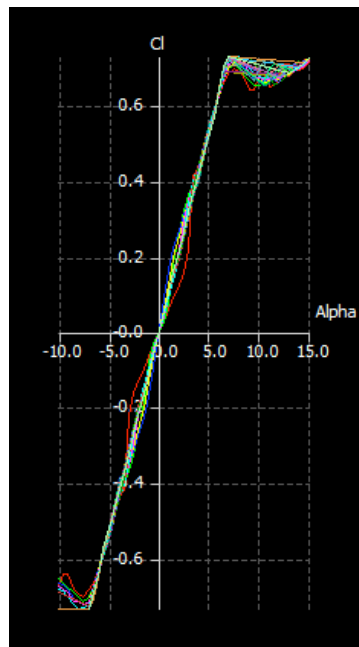


Figure 15: Lift Coefficient versus Angle of Attack for NACA 0008

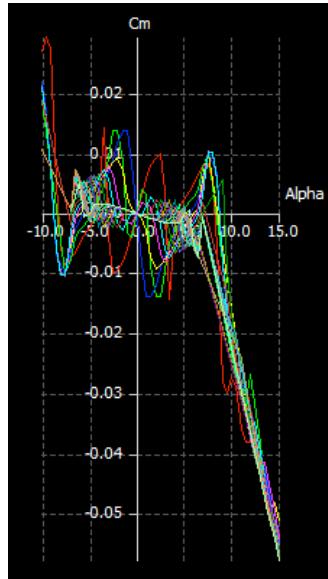


Figure 16: Moment Coefficient versus Angle of Attack for NACA 0008

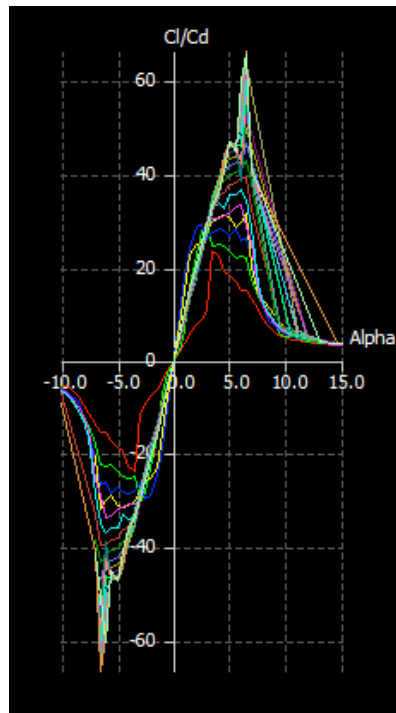


Figure 17: Lift/Drag Ratio versus Angle of Attack for NACA 0008

11.3 OTHER EMPENNAGE PARAMETERS

For the initial configuration, there will be a taper ratio of 1. There will be no sweep angle since there is a possibility of installing solar cells onto the empennage, which requires a large amount of available area. There will be no incidence angle because of a comparison of similar aircraft such as the SunSailor and Sky-Sailor.

11.4 DESIGN OF THE LONGITUDINAL AND DIRECTIONAL CONTROLS

For a v-tail empennage, there will need to be a combination rudder-elevator device, more commonly known as a “ruddervator,” on each side of the wing. Raymer suggests that a common length for ruddervators usually extends from the fuselage to about 90% of the tail span. For the solar-powered aircraft, it is better to extend the ruddervator all the way out to the tip for better control. Since there will be a taper ratio of 1 on the empennage itself, there will be the same taper ratio on the ruddervators. For the chord length of the ruddervators, Raymer suggests that 25-50% of the tail chord is sufficient. Therefore, 35% of the tail chord was chosen. A summary of the aileron sizing is shown in Table 8.

Table 8: Ruddervator Sizing (For One Ruddervator Only)

Ruddervator Length	0.7527 m
Ruddervator Chord	0.0846 m
Total Ruddervator Surface Area	0.0637 m ²

11.5 EMPENNAGE CAD DRAWINGS

The complete empennage CAD drawings were done using XFLR5 and the various views are shown in Appendix F.

11.6 COMPLETE AIRCRAFT CAD DRAWINGS

The fuselage, wing, and empennage were built using XFLR5, and an initial configuration using the dimensions from Sections 9, 10, and 11 was created. The various views of the aircraft are shown in Appendix G.

12.0 WEIGHT AND BALANCE

12.1 COMPONENT WEIGHT BREAKDOWN

One of the most vital components for a solar-powered aircraft is the batteries. The batteries not only must be lightweight, but also need to provide enough energy to supply power to the motor during flight. This is also how the aircraft's endurance is measured because with more batteries, you will be able to fly longer. However, weight then becomes an issue. For this aircraft, lithium-ion batteries were chosen because they provide more power than other types of batteries, and can be connected to motors fairly easily. The configuration is also important for sizing purposes and the amount of energy needed for the aircraft. Eight batteries in series will be connected in parallel to 5 other sets of 8 batteries. The common terminology for this type of configuration is 8S6P. Table 9 shows several lithium-ion batteries that were chosen. It is important to note that the battery with the highest energy density is preferable because with solar-powered

aircrafts, weight is more critical than power. In Table 9, the Panasonic NCR-18650A produces the highest energy density and will be used for this aircraft.

Table 9: Battery Specifications

Panasonic Batteries	NCR 18500	NCR 18650	NCR 18650 A
Nominal Voltage (V)	3.6	3.6	3.6
Nominal Capacity (Typical) (Ah)	2.0	2.9	3.1
Cell Configuration	8S6P	8S6P	8S6P
Cell Voltage (V)	28.8	28.8	28.8
Cell Capacity (Ah)	12.0	17.4	18.6
Cell Energy (Wh)	345.6	501.1	535.7
Cell Mass (kg)	1.61	2.16	2.18
Energy density (Wh/kg)	214.66	232.0	245.7

AzurSpace's S 32 cell was chosen for this aircraft because of its low weight and relatively high efficiency. It is also fairly flexible and can be connected to other components in the aircraft. The configuration for the separate solar panels will be 36 solar cells connected twice in series, totaling 72 solar cells for each solar panel. The maximum amount of solar panels that can be built is 11 since the maximum allowable area on the wing can only fit a total of 840 solar cells. With 11 solar panels, there will be 5 on each side of the wing and 1 located at the center of the wing.

To transfer the most energy from the solar panels to the batteries, a maximum power point tracker, or MPPT, must be used. There are different configurations for MPPTs. For business and home use, this device can be readily purchased at most stores

or anywhere solar panels can be purchased. However, for a solar-powered aircraft, these MPPTs are not ideal because of their weight. Since weight needs to be minimized for the MPPTs, it was decided that an MPPT will be built using a microcontroller and a processor unit. The issues with building such an MPPT are software capabilities as well as an understanding of microcontrollers. For this aircraft, Noth's model for a self-built MPPT will be used; the weight will also be taken into account.

The components that need power in the aircraft, such as motors, motor controllers, and GPS, will now be determined. The motor controller is a device that supplies power to the motor. The JETI JES 045 Plus DC speed controller will be used for this aircraft because it allows connections to lithium-ion batteries, and it has its own battery eliminator circuit, or BEC, which controls the amount of voltage that is supplied to the motor.

Brushless motors will be used because they provide more power than other electric model aircraft motors. It was decided to use an E-flite Power 90 Brushless Outrunner Motor 325Kv because it recommends a proper range of propellers for this aircraft, and it can be installed with the amount of battery cells that are on this aircraft.

The propeller's diameter was chosen to be a maximum of 16 inches, or 0.4064 meters, because of the fuselage size. Slight modifications were done to the fuselage as a result. The large fuselage diameter was changed from 0.4 m to 0.3 because there was a lot of unused room inside the fuselage and saving on weight is a priority. The motor and propeller's position was also changed so that they are higher than the center of the aircraft to provide enough clearance. There are two types of propellers that are currently

on the market: beechwood and APC. Beechwood is made of high-quality wood that is efficient. APC propellers are made from lightweight molded nylon, as well as other composites, to minimize drag and increase efficiency. For this aircraft, both propellers will be used and the one that will be used will depend on the amount of thrust it provides. The propeller pitch was chosen to be 8 inches. Therefore, a PJN Electric Beechwood Propeller and an APC 16'' x 8'' Competition Propeller will be analyzed.

The batteries will be connected to a series of microcontrollers and processing boards to supply power and direction to the servos and autopilot. These boards will primarily consist of dsPIC33 16-bit microcontrollers and digital signal controllers, as well as 8-bit PIC microcontrollers available from Microchip. Noth shows that the servo board, autopilot, and energy board can be built using these microcontrollers, and the Noth model will be used for the dimensioning of these boards and autopilot.

Once the boards are installed and connected correctly, the servo motors are then chosen. The servo motors will be brushless because they provide the best control for the aircraft. Futaba BLS154 Brushless Low Profile Servos will be used for the ailerons installed on the wing primarily because these can be installed easily. Futaba BLS151 Brushless Standard Air Servos will be used for the ruddervators installed on the empennage since these can be installed within the empennage and power can be supplied to them through the fuselage.

All other components, such as the GPS, RC Receiver, BECs, and the 3DOF Orientation Tracker, are based on Noth's model. Other components that can be neglected due to weight include an altimeter and an airspeed sensor. For both of these, the How

Fast Airspeed MPH instrument and the How High Model Aircraft Altimeter will be used. Since both of these together weigh less than 5 grams, they are ignored for the weight estimate analysis. Table 10 shows the component weights in detail.

Table 10: Component Weights

Component	Weight (in kg)
Batteries	2.18
Solar Panels	0.6
MPPT	0.1
Motor Controller	0.026
Motor	0.45
Propeller	0.036
Servos	0.19
Microcontroller Boards (Autopilot, Energy Board, Servo Board)	0.04
Other (GPS, RC Receiver, IMU, Wiring, etc.)	0.2
TOTAL	3.822

The values obtained from Table 10 will allow up to 3.91 kg for the airframe for both the fuselage and the wing in order to meet our weight restrictions. It is difficult to determine how much the airframe will weigh without building the aircraft. However, while using composites and other lightweight materials, the airframe should not exceed 4 kg. Comparing these results with Table 5 shows that the largest difference is the battery

weight, and the other calculations for the propulsion group, avionics, etc., remain the same. Therefore, Noth's estimation model can be used as an initial approximation for building a solar-powered aircraft.

12.2 CENTER OF GRAVITY CALCULATIONS AND DISCUSSION

Now that the weights for each component have been determined in Section 12.1, the center of gravity for various loading scenarios will be calculated. For the fuselage and the wing weights, the estimated airframe structure weight for each will be included. From Section 12.1, there is 3.91 kg left for the structure of the entire aircraft. This amount will be divided among each airframe section of the aircraft will be assumed to be a certain percentage of the total airframe weight. The weights then become 1.955 kg for the large fuselage structure, 0.6517 kg for the small fuselage structure, 0.9775 kg for the wing structure, and 0.3258 kg for the empennage structure.

The exact dimensions of the aircraft will need to be known before the center of gravity is calculated. Figures 18 and 19 show the components and dimensions of the aircraft. For the top and front views of the aircraft, please see Appendix H. Table 11 shows the calculated values of the center of gravity location for each component. It is important to note that there are two loading scenarios: the aircraft with no payload and the aircraft with a full payload. Any payload weight that is between 0 and 2.268 kg will cause the aircraft to have a center of gravity between the two extreme cases.

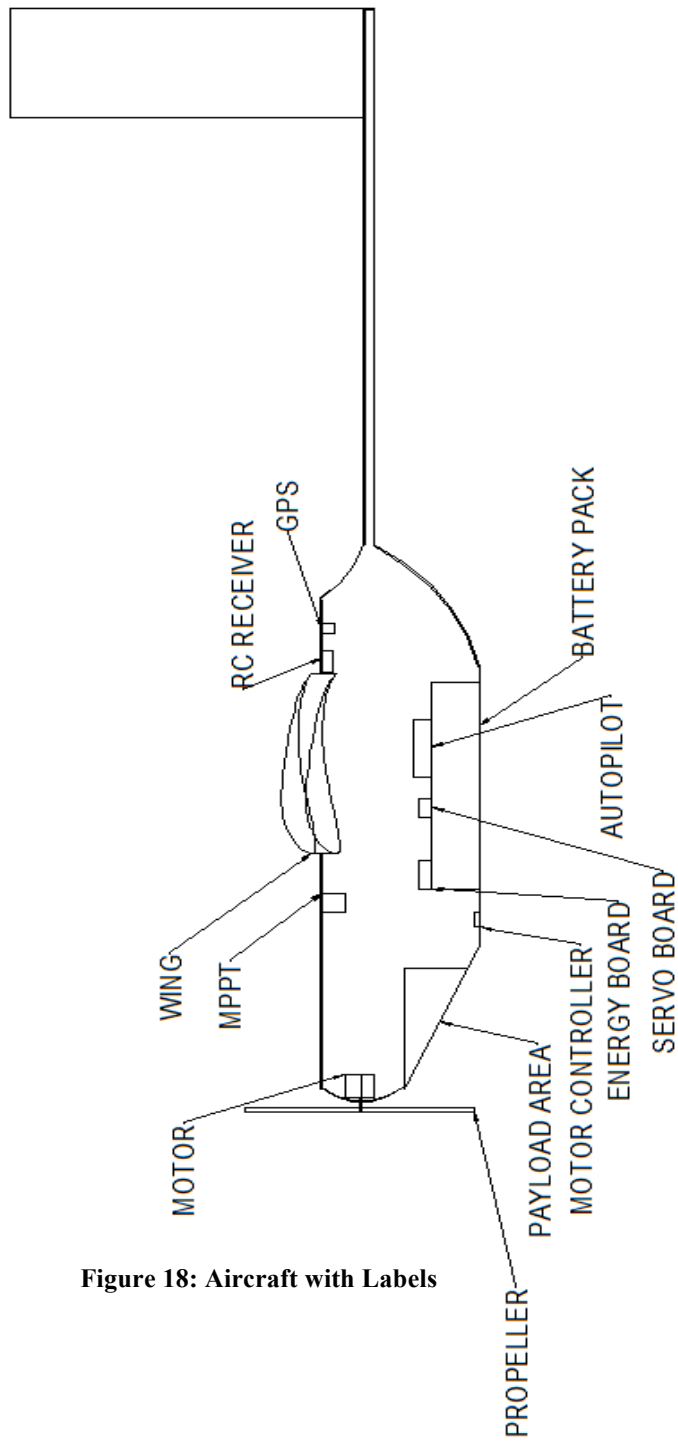


Figure 18: Aircraft with Labels

Table 11: Center of Gravity Locations

Component	Center of Gravity Location from Nose of Aircraft (in cm)	Weight (in kg)
Propeller	-1.29	0.036
Motor	3.81	0.45
Payload	19.62	2.268
MPPT	44.94	0.1
Motor Controller	41.09	0.026
Energy Board	49.99	0.015
Servo Board	66.14	0.01
Autopilot	79.39	0.015
Battery Pack	71.06	2.18
Wing (includes servos, airframe, and solar panels)	66.06	1.6775
RC Receiver	99.17	0.01
GPS	106.58	0.01
Large Fuselage Structure	62.64	1.955
Small Fuselage	185.29	0.6517
Empennage	227.11	0.4158
TOTAL WITH PAYLOAD	66.04	10
TOTAL WITHOUT PAYLOAD	61.59	7.732

A safe assumption that will be used is that the center of lift acts at the quarter-chord point of the wing. The distance from the nose of the aircraft to the center of lift then becomes 66.0564 cm. Comparing this number with the center of gravity calculation for the entire aircraft with and without payload, the center of gravity is ahead of the center of lift in both cases. This is ideal because this allows the aircraft to be statically stable. Also, the static margin when the aircraft has no payload is 11.1%, which is comparable with other model R/C aircraft. Therefore, this aircraft would not need any stability augmentation system.

13.0 STABILITY AND CONTROL ANALYSIS

13.1 STATIC LONGITUDINAL STABILITY

The static longitudinal stability will be based on the methods of Roskam from parts III, V, and VI. To find the ideal horizontal stabilizer area for a certain static margin, a longitudinal X-plot is used. The center of gravity graph is based on the Cessna method from Raymer, Part V, and is shown in (13.1):

$$W_h = \frac{3.184(W_{TO})^{0.887}(S_h)^{0.101}(A_h)^{0.138}}{57.5(t_{r_h})^{0.223}} \quad (13.1)$$

The horizontal stabilizer area is the independent variable in (13.1), so a relationship between horizontal stabilizer area and weight is determined. Using the constant weights from Section 12, the relationship between the location of the center of gravity per unit chord length and horizontal stabilizer area can be determined.

To calculate the location of the aerodynamic center per unit chord, methods shown in Roskam Part III will be used to determine the relationship between horizontal stabilizer area and aerodynamic center. These are shown in (13.2) and (13.3):

$$\bar{x}_{ac_A} = \frac{\bar{x}_{ac_{wf}} + \frac{C_{L_{oh}} \left(1 - \frac{\partial \epsilon_h}{\partial \alpha}\right) \left(\frac{S_h}{S}\right) \bar{x}_{ac_h}}{C_{L_{ovf}}}}{F} \quad (13.2)$$

$$F = 1 + \frac{C_{L_{oh}} \left(1 - \frac{\partial \epsilon_h}{\partial \alpha}\right) \left(\frac{S_h}{S}\right)}{C_{L_{ovf}}} \quad (13.3)$$

The wing-fuselage lift curve slope can be solved with (13.4):

$$C_{L_{ovf}} = k_{wf} C_{L_{ov}} \quad (13.4)$$

The wing-fuselage coefficient is determined by an empirical method using the wingspan and equivalent fuselage diameter from (13.5):

$$k_{wf} = 1 + 0.025 \left(\frac{d_f}{b}\right) - 0.25 \left(\frac{d_f}{b}\right)^2 \quad (13.5)$$

The wing lift curve slope using Roskam Part VI is simplified since most of the variables do not apply to the aircraft. Thus, the wing lift curve slope can be solved using (13.6):

$$C_{L_{ov}} = \frac{2\pi A}{2 + \left[\left(\frac{A^2 \beta^2}{k^2} \right) + 4 \right]^{1/2}} \quad (13.6)$$

To find the Mach constant, (13.7) is used with the maximum cruise speed converted to Mach number:

$$\beta = (1 - M^2)^{1/2} \quad (13.7)$$

To calculate the Mach variable, (13.8) is used:

$$k = \frac{(C_{l\alpha})_M}{\frac{2\pi}{\beta}} \quad (13.8)$$

To determine the airfoil lift curve slope at the maximum cruise speed, Figure 15 was used from XFLR5. To calculate the horizontal lift curve slope, replace (13.6) with values applicable to the horizontal stabilizer such as the aspect ratio and the airfoil lift curve slope. To calculate the downwash gradient at the horizontal tail, Roskam's methods are used and then simplified again for this aircraft, and is shown in (13.9):

$$\frac{\partial \varepsilon_h}{\partial \alpha} = 4.44(K_A K_h)^{1.19} \quad (13.9)$$

The aspect ratio coefficient that is required in Eq. (13.9) can be found from (13.10):

$$K_A = \frac{1}{A} - \frac{1}{1 + A^{1.7}} \quad (13.10)$$

The horizontal stabilizer coefficient, using the geometry from Roskam, can be found using (13.11):

$$K_h = \frac{1 - \frac{h_h}{b}}{\left(\frac{2l_h}{b}\right)^{1/3}} \quad (13.11)$$

In Eq. (13.11), all quantities will be measured from the nose of the aircraft as the x-component and from the mean chord for the y-component. Equations (13.2) through (13.11) were put in a MATLAB code and the code is attached in Appendix C.5. Figure 20 shows the results. Assuming a 10% static margin which is common for most aircraft, then the required horizontal stabilizer area from Figure 20 becomes 9.3 ft², or 0.864 m². In Section 11, it was shown that the horizontal stabilizer area for an initial configuration was 0.2953 m². One reason why these values are different is because of the Cessna method, which is used for general light aircraft, but not model aircraft. Even though the stability and control analysis requires this large of area, the original area from Section 11 will be used since comparable aircraft can also fly with a similar empennage area. The longitudinal X-plot suggests that the distance from the tip of the nose to either the aerodynamic center or the center of gravity of the aircraft is about 2.1 times the wing chord length, or about 80 cm. In Section 12, when including each individual component of the aircraft, the center of gravity was about 1.5 times the wing chord length. Since Section 12 considered each individual component of the aircraft carefully, the center of gravity location from Section 12 will be used.

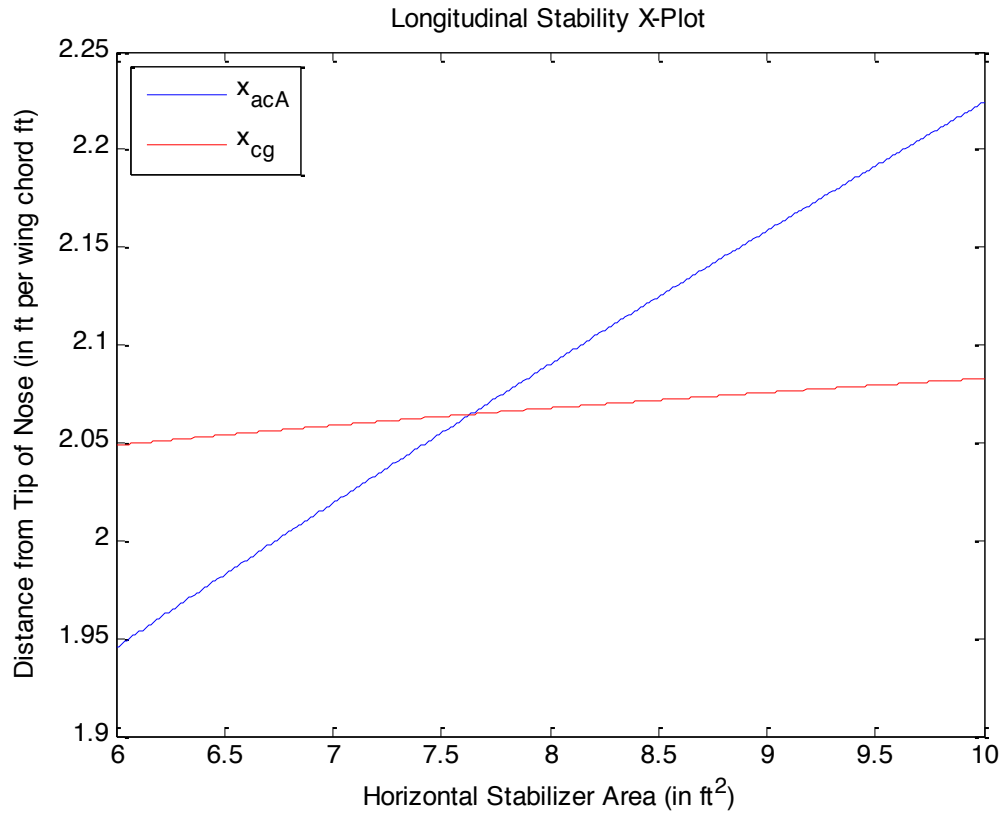


Figure 20: Longitudinal Stability X-Plot

13.2 STATIC DIRECTIONAL STABILITY

A relationship between the yaw side-slip moment coefficient and the horizontal stabilizer area can be determined using (13.12):

$$C_{n_\beta} = C_{n_{\beta_{vf}}} + C_{L_{av}} \left(\frac{S_v}{S} \right) \left(\frac{x_v}{b} \right) \quad (13.12)$$

Since the yaw side-slip wing coefficient is assumed to be zero at high angle of attack, the assumption that the yaw side-slip wing-fuselage coefficient is equal to the yaw side-slip fuselage coefficient can be used, and the yaw side-slip fuselage coefficient is defined in (13.13):

$$C_{n_{\beta}} = -57.3K_N \left(\frac{S_{f_s} l_f}{Sb} \right) \quad (13.13)$$

Roskam uses 0.0015 as the value of K_N and that value will be used for this analysis. The geometry from Figure 19 will be used to determine geometrical constants in (13.12) and (13.13). Also, since the empennage is a v-tail configuration, the vertical lift curve slope is the same as the horizontal lift curve slope that was calculated in Section 13.1. The variables and equations were put into the same MATLAB code described in Section 13.1, and Figure 21 shows the directional stability x-plot. When the yaw side-slip moment coefficient is equal to 0.001, the recommended vertical stabilizer area is 2.92 ft², or 0.27 m². In Section 11.1, the calculated vertical stabilizer area was determined to be 0.1536 m², which is about half of the recommended area from the stability and control analysis. The calculated vertical stabilizer area from Section 11.1 will be used since other R/C model aircraft use a similar size for their v-tail and are capable of directional stability.

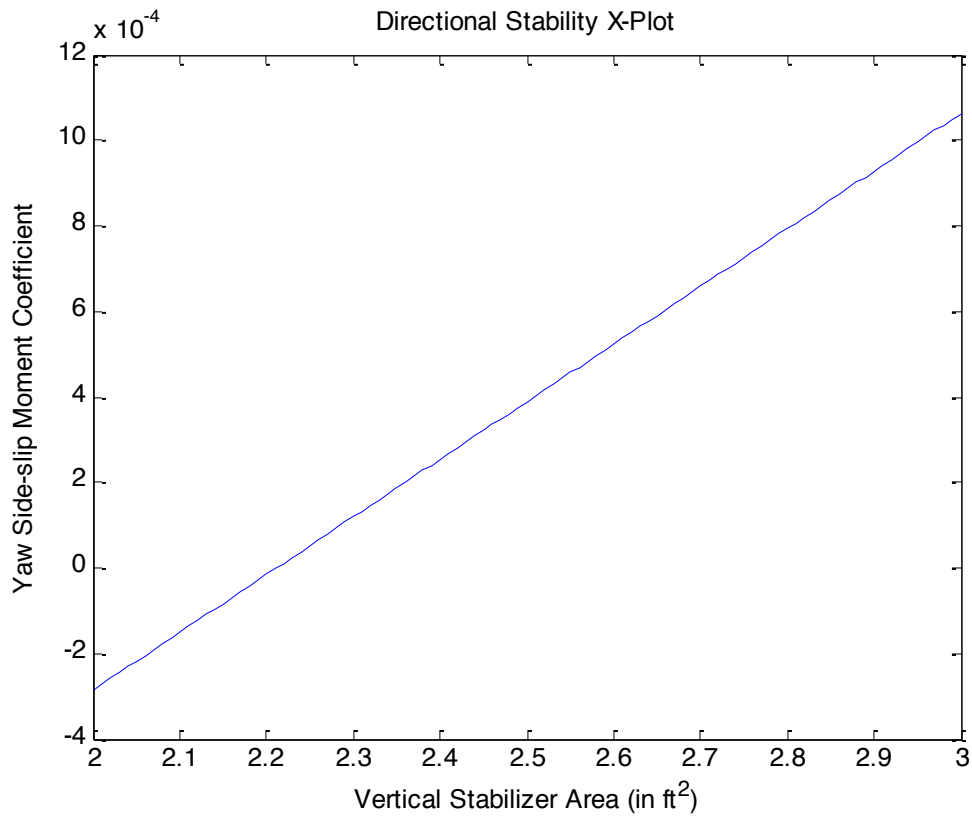


Figure 21: Directional Stability X-Plot

14.0 DRAG POLAR ESTIMATION

14.1 AIRPLANE ZERO LIFT DRAG

The airplane's zero lift drag calculation will be based on Roskam Part II methods of a Class 1 drag polar estimation. The total wetted area of the aircraft will be calculated using (14.1), which is a simplified equation from Roskam that is specific to this aircraft:

$$S_{wet,w} = 2S_{wing} \left[1 + 0.25 \left(\frac{t}{c} \right)_r \right] \quad (14.1)$$

Knowing the maximum thickness of the Selig 1223 airfoil is 12.1%, and the total wing area converted in ft^2 is 22.712, the total wing wetted area can be calculated:

$$S_{wet,w} = 2(22.712 ft^2)[1 + 0.25(0.121)] = 46.8 ft^2$$

For the empennage, (14.1) will be used, but specific to the horizontal and vertical tail areas. The total empennage area when summing the horizontal and vertical tail areas is $4.833 ft^2$. Since a NACA 0008 airfoil will be used for the entire empennage, the maximum thickness of the airfoil is 8%. The total empennage wetted area can be calculated:

$$S_{wet,e} = 2(4.833 ft^2)[1 + 0.25(0.08)] = 9.86 ft^2$$

The fuselage wetted area can be calculated using (14.2):

$$S_{wet,f} = \pi D_f l_f \left(0.5 + 0.135 \frac{l_n}{l_f} \right)^{2/3} \left(1.015 + \frac{0.3}{\lambda_f^{1.5}} \right) \quad (14.2)$$

Using the geometry provided in Figure 19, the total fuselage wetted area can be solved for:

$$S_{wet,f} = (3.14)(0.98 ft)(8.04 ft) \left(0.5 + 0.135 \frac{1.15 ft}{8.04 ft} \right)^{2/3} \left(1.015 + \frac{0.3}{8.2^{1.5}} \right) = 16.44 ft^2$$

Since there are no flaps or slats, or any other areas that are needed to account for, the entire airplane's wetted area can now be determined:

$$S_{wet,tot} = S_{wet,w} + S_{wet,e} + S_{wet,f} = 46.8 + 9.86 + 16.44 = 73.1 ft^2$$

To calculate the equivalent parasite area, Roskam's methods will be used. Using the largest skin friction coefficient of 0.01 from Roskam, the equivalent parasite area using the calculated wetted area is $0.731 ft^2$. The clean zero-lift drag coefficient can now be determined using (14.3):

$$C_{D_o} = \frac{f}{S_{wet,tot}} \quad (14.3)$$

Using the value for the parasite area and wetted area, the clean zero-lift drag coefficient becomes 0.01.

14.2 AIRPLANE DRAG POLAR

The drag polar will now be calculated for the airplane itself. Using the value of the calculated zero-lift drag coefficient, the overall aircraft drag coefficient can be calculated using (14.4):

$$C_D = C_{D_o} + \frac{C_L^2}{\pi e AR} \quad (14.4)$$

Assuming a lift coefficient of 1.5 from Section 8.3, as well as an Oswald efficient factor of 0.9, the total aircraft drag coefficient can be calculated:

$$C_D = 0.01 + \frac{1.5^2}{(3.14)(0.9)(13)} = 0.0712$$

Assuming that the lift coefficient stays constant, the lift-to-drag ratio of the aircraft can be calculated as follows:

$$\frac{L}{D} = \frac{C_L}{C_D} = \frac{1.5}{0.0712} = 21.06$$

In Section 8.3, Noth's model was used to calculate the drag coefficient, and it was determined that the total drag coefficient of the aircraft was 0.0967. This gives a lift-to-drag ratio of 15.5. One final drag polar determination was found using the XFLR5 program, which was also used for the airfoil analyses in the previous sections. Within XFLR5, an aircraft can be designed and flight conditions can be inputted, and the software will calculate the lift and drag coefficients at a given angle of attack. The software uses the vortex lattice method and the assumptions that go along with this method. The input parameters for the aircraft were based on the geometry for the initial configuration, as well as an altitude of 2,000 m and the maximum cruise speed of 13.5 m/s. The result of the XFLR5 analysis that shows the drag polar is shown in Appendix I. From this analysis, the highest lift-to-drag ratio occurs at an angle of attack of 0.5 degrees, and is 17.72. The lift and drag coefficients for this case are 1.0143 and 0.0572 respectively. The drag polar results are shown in Table 12.

Table 12: Drag Polar Comparison

	Section 8.3 Analysis (Old)	Section 14.2 Analysis (New)	XFLR5 Analysis
Lift Coefficient	1.5	1.5	1.0143
Drag Coefficient	0.0967	0.0712	0.0572
Lift-to-Drag Ratio	15.5	21.06	17.72

14.3 DISCUSSION

The drag polar results in Table 12 show that the lift-to-drag ratio ranges from 15.5 to 21.06. The main difference between the Section 8.3 and Section 14.2 analysis is the drag coefficient. The Section 8.3 analysis was taken from Noth and assumes that there is a fuselage drag coefficient added to the total drag coefficient. The XFLR5 analysis shows that there is a lower lift coefficient when compared to the other two analyses, but there is also a lower drag coefficient. That is why the lift-to-drag ratio for the XFLR5 analysis is between the other two analyses. It is hard to determine which one of these analyses is the most accurate since a prototype has not been built yet. However, since the Section 14.2 analysis does not include the fuselage drag coefficient and the others include that, that analysis is the most inaccurate. If there was the capability within XFLR5 to better define the aircraft, then it would be the most accurate. The XFLR5 result will be used for future analysis if needed.

15.0 ENVIRONMENTAL / ECONOMIC TRADEOFFS

15.1 ENVIRONMENTAL ISSUES

The environmental issues that are related to this solar-powered UAV are few when compared to a commercial aircraft or model aircraft that uses fuel. However, there are still several issues faced. First, the battery and other materials within the aircraft are toxic and are harmful to the environment if the aircraft crashed suddenly or crashed into the ocean. If the aircraft and all materials are not disposed of properly, this could harm the environment. Another issue is the fact that our aircraft is a zero fuel emission aircraft, which means that no gasoline or other oil-based fuel, like bio-fuels, is used. Fuel emissions release carbon dioxide into the atmosphere and increase the chlorofluorocarbons. This is important because it will then increase the greenhouse effect, which will then increase the global surface temperature of the Earth. In 1975, Ramanathan [13] did a study that showed that if the global surface temperature increased by 0.5°K , then there will be significant changes across the globe, including an increase in water height due to polar ice caps melting and changes in crops and rainfall. Therefore, it is important that carbon emissions are reduced to keep the environment the same.

These issues were not relevant 25 or 50 years ago because many people did not study how the effect of the industrial age would impact the environment around us. In the last 10-15 years however, there has been a heavy concentration on reducing emissions and recycling. With the invention and popularity of hybrid vehicles, this has greatly reduced the emissions from motor vehicles. However, zero emission vehicles have yet to gain enough popularity in our world. In regards to aircraft specifically, the idea of a zero

emission aircraft is still not considered since there still needs significant advances in technology. Bio-fuels for commercial aircraft have been gaining some popularity, and hydrogen fuel cells are being looked at for aircraft, but both of these still use some sort of limited energy to power the aircraft. Solar energy not only is free of emissions, but as the efficiency of the solar cell increases, you can potentially have an aircraft that flies high enough so that it receives the Sun's energy for a long period of time, such as months or years, all powered with solar cells.

15.2 ECONOMIC TRADEOFFS

The increase in fuel costs over the last few years drive an alternative source of energy, whether it is bio-fuels, hydrogen fuel cells, or solar cells. Bio-fuels have the advantage currently because more funding was put in this technology by aviation companies than any other alternative source of energy. The other reason why bio-fuels were chosen is because it would be simple to implement them in current commercial aircraft, which would save money since a new aircraft would not have to be built. However, they are the most expensive over time when compared to hydrogen fuel cells or solar cells because commercial aircraft would use millions of pounds of this fuel over the next 50 years or so. There will come a point in time where it would be cheaper to build entirely new aircraft with solar technology than to use bio-fuels. Therefore, not only will solar technology be better for the environment, but it will also be more cost-effective over a long period of time when compared to current commercial aircraft fuel.

15.3 SOLUTIONS

The ideal solution would be to build a similar commercial aircraft, like a Boeing 787, using only zero emissions technology, such as solar cells. Currently, the efficiency of the solar cells are too low to make this happen, but over a long period of time, the efficiency will increase to a point where larger commercial aircraft could use solar cells to power the entire aircraft. With the Solar Impulse, it was shown that manned aircraft can fly using only solar technology. Therefore, commercial solar-powered aircraft could realistically be seen within the next 50 years.

16.0 CONCLUSIONS / RECOMMENDATIONS

With the current desire for a greener society, an alternative source of energy for aircraft is needed. There are many alternative energy solutions that are promising, including bio-fuel and hydrogen fuel cells, but nothing is as limitless as solar technology. The application of small solar-powered UAVs can potentially be very large, whether it is in weather surveillance, studying natural disasters, or fire detection. The solar-powered design discussed weighs no more than 10 kg, has a wingspan of less than 7 m, and hold up to 2.27 kg of payload, which is enough for any surveillance equipment needed to investigate fires. The advances in solar technology have made it so the concept of solar-powered UAVs and MAVs is not just a theory anymore. Solar-powered aircraft can be an important part of the future of aviation, and can be a solution to a greener society.

REFERENCES

- [1] The History of Solar, U.S. Department of Energy, Energy Efficiency and Renewable Energy [Online]. Available: http://www1.eere.energy.gov/solar/pdfs/solar_timeline.pdf.
- [2] A. Noth, "History of Solar Flight," Autonomous Systems Lab, Switzerland: ETH Zürich, 2008.
- [3] Solar Impulse Project, Wikipedia. Available: http://en.wikipedia.org/wiki/Solar_Impulse_project.
- [4] A Weider, H. Levy, I. Regev, L. Ankri, T. Goldenberg, Y. Ehrlich, A. Vladimirsky, Z. Yosef, M. Cohen, (2006). SunSailor: Solar Powered UAV, Technion IIT, Haifa, Israel .
- [5] C.L. Nickol, M.D. Gynn, L.L. Kohout, T.A. Ozoroski, (2007, March). High Altitude Long Endurance UAV Analysis of Alternatives and Technology Requirements Development, *NASA/TP-2007-214861*. Available: NASA Technical Reports Server.
- [6] T. Tegeder, "Development of an Efficient Solar Powered Unmanned Aerial Vehicle with an Onboard Solar Tracker," M.S. Thesis, Brigham Young University, Utah, 2007.
- [7] N. Baldock, M.R. Mokhtarzadeh-Dehghan, (2006). A Study of Solar-Powered, High-Altitude Unmanned Aerial Vehicles, *Aircraft Engineering and Aerospace Technology: An International Journal*, 78(3), pp. 187-193.
- [8] DARPA's Vulture Program Enters Phase II, Defense Advanced Research Projects Agency. Available: <http://www.darpa.mil/news/2010/NewsReleaseVultureII.pdf>.
- [9] D.P. Raymer, *Aircraft Design: A Conceptual Approach*. 2nd Ed., AIAA Education Series, 1992.
- [10] J. Roskam, *Airplane Design Parts I-VIII*. Roskam Aviation and Engineering Corporation, Route 4, Box 274, Ottawa, Kansas, 1985-1990.
- [11] A. Noth, "Design of Solar Powered Airplanes for Continuous Flight," Ph.D. dissertation, ETH Zürich, Switzerland, 2008.

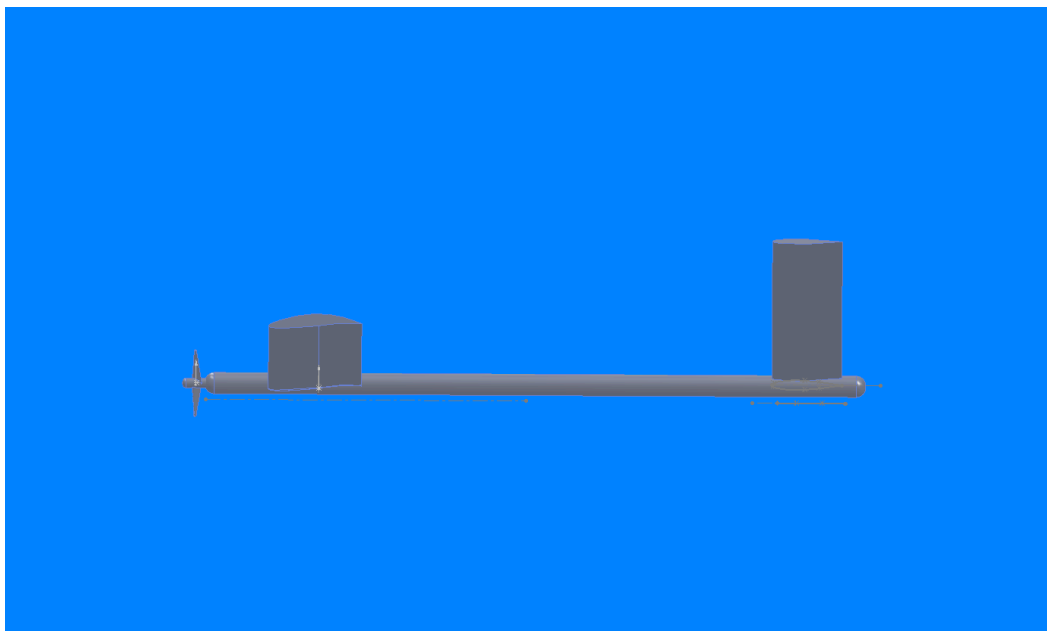
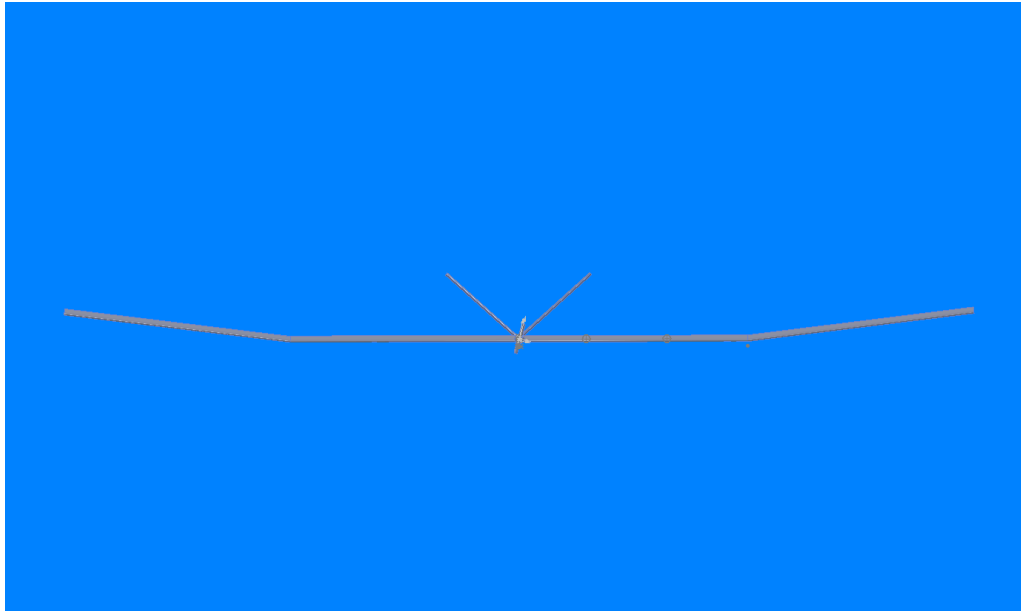
- [12] Calculation of Solar Insulation, PVCDROM. Available:
<http://pvcdrom.pveducation.org/index.html>.
- [13] V. Ramanathan, (1975). Greenhouse Effect Due to Chlorofluorocarbons: Climatic Implications. *Science New Series*, 190(4209), pp. 50-52.

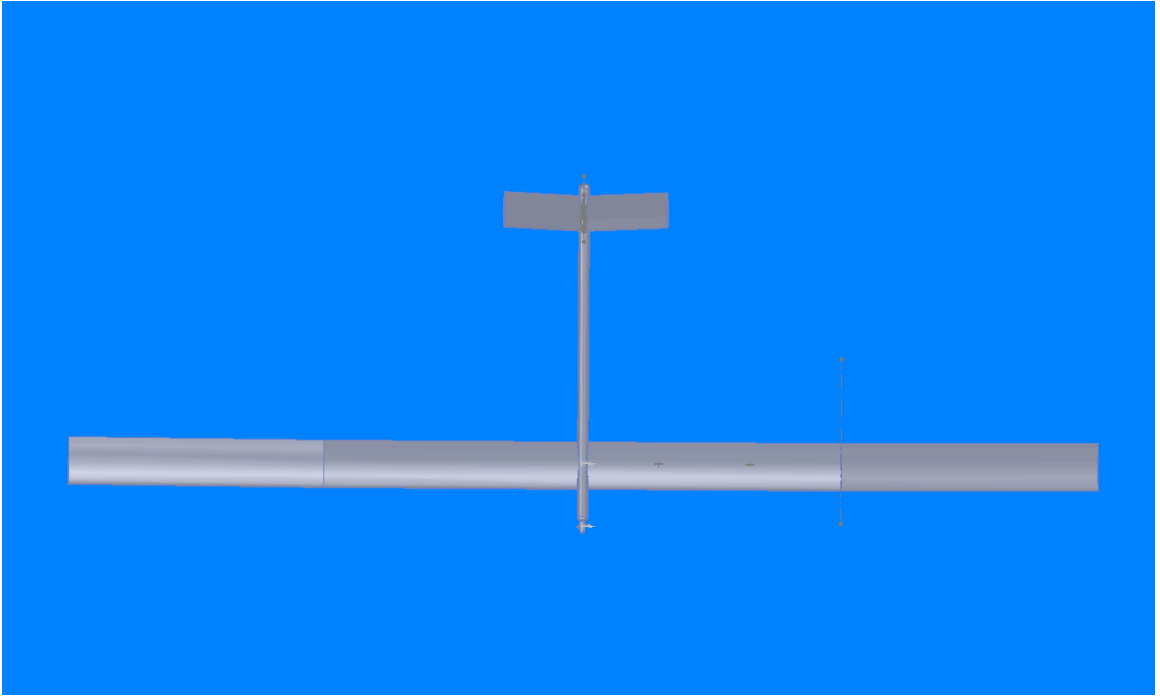
APPENDICES

Appendix A: Complete Design Parameters for Similar Aircraft

	Sunrise I	Sunrise II	Solar Solitude	Solar Excel	SoLong	Zephyr	SunSailor 1/2
Weight (in kg)	12.25	10.21	2	0.72	12.6	50	3.6
Endurance	4 hours	Unknown	Unknown	11 hours, 34 minutes, 18 seconds	48 hours, 16 minutes	336 hours, 21 minutes (14 days)	Unknown
Range	Unknown	Unknown	38.84 km in a straight line	48.31 km in a straight line	Control and telemetry range: 8 km	Unknown	139 km
Wingspan (in m)	9.75	9.75	2.7	2.1	4.75	22.5	4.2
Aspect Ratio	11.4	11.4	13.3	12.8	15	11.6	13.15
Wing Area (in m ²)	8.36	8.36	0.55	0.35	1.5	27.9	1.35
Cruise Altitude	Unknown	Unknown	Max altitude = 1283 m	2065 m	Unknown	Max is 70,000 ft. Climbs to 40,000 ft on first day, then maintains 60,000 ft.	Max is 500 ft above ground level due to restrictions
Cruise Velocity	Unknown	Unknown	Unknown	Max velocity = 80.63 km/hr	27-50 mph	Unknown	25 knots
Max Climb Rate	Unknown	Unknown	Unknown	Unknown	2.5 m/s	Unknown	300 ft/min

Appendix B: Front, Size, and Top Views for Initial Configuration





Appendix C: Matlab M-Files for Solar-Powered Aircraft Analysis

Appendix C.1: InitParameters2.m

```
% Global Design of Sky-Sailor Airplane
% Initialization of Parameters
% A.Noeth, 2008

g          = 9.81;          % Gravitational acceleration (m/s^2)
alt        = 2000;         % Initial altitude (m)
alt_array  = [0, 1000, 2000, 4000, 6000, 10000, 15000, 20000,
25000, 30000];
rho_array  = [1.224, 1.11, 1.006, 0.819, 0.659, 0.413, 0.192,
0.087, 0.039, 0.017];
rho        = spline(alt_array,rho_array,2000); %Airdensity at
2000m [kg/m^3]

% Irradiance conditions

I_max      = 1040;         % Maximum irradiance [W/m^2]
T_day      = 14*3600;     % Duration of the day [s]
n_wthr     = 0.7;         % Margin factor <1 take clouds into
account

% Aerodynamics
C_L        = 1.5;         % Airfoil lift coefficient
C_D_afl    = 0.029;      % Airfoil drag coefficient
C_D_par    = 0.0065;     % Fuselage drag coefficient
e          = 0.9;         % Constant depending on wing shape

% Wing and fuselage Structures
k_af       = 0.44/9.81/5; % Constant [Kg/m3]
x1         = 3.1;         % Scaling exponent for b
x2         = -0.25;      % Scaling exponent for AR

% Propulsion group
n_ctrl     = 0.95;       % Efficiency of motor controller
n_mot      = 0.85;       % Efficiency of motor
n_grb      = 0.97;       % Efficiency of gearbox
n_plr      = 0.85;       % Efficiency of propeller
k_prop     = 0.008;      % Mass/Power ratio of propulsion
group [kg/W]

% Battery and Stepdown converter
n_chrg     = 0.95;       % Efficiency of charge process
n_dchrg    = 0.95;       % Efficiency of discharge process
n_bec      = 0.65;       % Efficiency of bec (5V stepdown)
k_bat      = 190*3600;   % Energy density of LiPo [J/Kg]

% Solar cells
k_sc       = 0.32;       % Mass density of solar cells [Kg/m2]
```

```

k_enc          = 0.26;          % Mass density of encapsulation
[Kg/m2]
k_mppt         = 1/2368;        % Mass/Power ratio of mppt [kg/W]
n_sc           = 0.169;        % Efficiency of solar cells
n_cbr          = 0.9;          % Efficiency of cambered
configuration
n_mppt         = 0.97;         % Efficiency of mppt

% Avionics and Payload
m_av           = 1;            % Mass of controller and electronics
[kg]
m_pld          = 2.268;        % Mass of payload [kg]
p_av           = 1.5;          % Power required for control [W]
p_pld          = 0;            % Power required for payload [W]

```

Appendix C.2: EvaluateSolution.m

```

% Global Design of Sky-Sailor Airplane
% Evaluation of the solution
% A.Noth, 2008

C_D_ind          = C_L^2 / (e*pi*AR);          % Induced drag
coefficient
C_D              = C_D_afl+C_D_ind+C_D_par;    % Total drag
coefficient

a0 = C_D/(C_L^1.5)*sqrt(2*AR*(g^3)/rho);      % Eq 3.5
a1 = 1/(n_ctrl * n_mot * n_grb * n_plr);      % Eq 3.6
a2 = 1/(n_bec)*(p_av+p_pld);                  % Eq 3.6
a3 = m_av + m_pld;                            % Eq 3.10
a4 = k_af*AR^x2;                              % Eq 3.25
a5 = k_sc + k_enc;                            % Eq 3.27
a6 = k_mppt * I_max * n_sc * n_cbr * n_mppt;  % Eq 3.28
a7 = T_night/(n_dchrg * k_bat);              % Eq 3.30
a8 = k_prop;                                  % Eq 3.32
a9 = pi/(2*n_sc*n_cbr*n_mppt*n_wthr) *
(1+T_night/(T_day*n_chrg*n_dchrg))*1/I_max;  % Eq 3.26
a10 = a0 * a1*(a7 + a8 + a9*(a5 + a6));        % Eq 3.34
a11 = a2 * (a7 + a9*(a5+a6))+a3;              % Eq 3.34
a12 = a10 * 1/b;                             % Eq 3.35
a13 = a11+a4*b^x1;                           % Eq 3.35

z = roots([a12 -1 0 a13]);                    % Solving equation to
find mass
Sol_m = MinimumPositive(z)^2;                 % It can be 2 masses,
we take the smallest one

if (isnan(Sol_m)==0)                          % If a solution is
found, we compute ...
    Sol_P_level = a0*Sol_m^1.5/b;              % Eq 3.5 level flight
power
    Sol_m_af = a4*b^x1;                       % Eq 3.25 airframe
mass
    Sol_P_elec_tot = a1*Sol_P_level+a2;        % Eq 3.6 total
electric power (level flight)
    Sol_m_bat = a7*Sol_P_elec_tot;            % Eq 3.30 battery mass
    Sol_A_sc = a9*Sol_P_elec_tot;            % Eq 3.26 solar panels
area
    Sol_m_sc = a5*Sol_A_sc;                  % Eq 3.27 solar panels
mass
    Sol_m_mppt = a6*Sol_A_sc;                % Eq 3.28 mppt mass
    Sol_P_sc = a6*Sol_A_sc/k_mppt;          % Eq 3.28 solar
electrical power max
    Sol_m_prop = a8*a1*Sol_P_level;          % Eq 3.32 propulsion
group mass
    Sol_v = sqrt(2*Sol_m*g/(C_L*rho*b*b/AR)); % Eq 3.3 level
flight speed

```

```

        Sol_D          = Sol_m*g/C_L*C_D;          % Eq. 3.1-2 total drag
        Sol_A          = b^2/AR;                  % wing
surface
end

if ((isnan(Sol_m)==1) || (Sol_A_sc > b*b/AR))    % If no solution,
Nan is returned
    Sol_m              = NaN;
    Sol_P_level        = NaN;
    Sol_m_af           = NaN;
    Sol_P_elec_tot     = NaN;
    Sol_m_bat          = NaN;
    Sol_A_sc           = NaN;
    Sol_m_sc           = NaN;
    Sol_m_mppt         = NaN;
    Sol_P_sc           = NaN;
    Sol_m_prop         = NaN;
    Sol_v              = NaN;
    Sol_D              = NaN;
    Sol_A              = NaN;
end

```

Appendix C.3: Function MinimumPositive.m

```
function min_pos = MinimumPositive(z)

min_pos = NaN;
for j=1:1:length(z)
    if (isreal(z(j)) && z(j)>0)
        if isnan(min_pos)
            min_pos = z(j);
        elseif z(j) < min_pos
            min_pos = z(j);
        end
    end
end
end

end
```

Appendix C.4: Main.m

```
% Global Design of Sky-Sailor Airplane
% Plot Example for Unmanned Aerial Vehicle
% A.Noth, 2008

clc;clear;clf;
cmap      = colormap(gray(100));
j        = 0;

InitParameters2;
T_night   = 24*3600-T_day;

for AR = [8,9,10,11,12,13,14,15,16,18,20]
    j      = j+1;
    col    = cmap(floor(((100-20)-0)/(20-8)*(AR-8))+1,:);

    i      = 0;
    b_max  = 25;
    b_step = .1;

    for b=b_step:b_step:b_max
        EvaluateSolution;
        i      = i+1;
        m(i)   = Sol_m;
        P_level(i) = Sol_P_level;
        m_af(i) = Sol_m_af;
        P_elec_tot(i) = Sol_P_elec_tot;
        m_bat(i) = Sol_m_bat;
        A_sc(i) = Sol_A_sc;
        m_sc(i) = Sol_m_sc;
        m_mppt(i) = Sol_m_mppt;
        P_sc(i) = Sol_P_sc;
        m_prop(i) = Sol_m_prop;
        v(i) = Sol_v;
        D(i) = Sol_D;
        A(i) = Sol_A;
    end

    width = 2;
    b = b_step:b_step:b_max;

    figure(1);set(gcf,'Position',[1056 204 560 420]);
    hold on;
    plot(b,m,'Color',col,'LineWidth',width);
    [m_min.m(j),index] = min(m);
    m_min.b(j)=b(index);
    grid on;
    xlabel('Wingspan [m]');
```

```

        ylabel('Total Mass of Solar Airplane [Kg]');

figure(2);set(gcf,'Position',[487 704 800 420]);
subplot(2,2,1);hold on;
    plot(b,v,'Color',col,'LineWidth',width);
    [v_min.v(j),index] = min(v);
    v_min.b(j)=b(index);
    grid on;
    ylabel('Speed [m/s]')
subplot(2,2,3);hold on;
    plot(b,P_level,'Color',col,'LineWidth',width);
    grid on;
    xlabel('Wingspan [m]');
    ylabel('Power at propeller [W]')
subplot(2,2,2);hold on;
    plot(b,A,'Color',col,'LineWidth',width);
    grid on;
    ylabel('Wing Area [m^2]')
subplot(2,2,4);hold on;
    plot(b,A_sc./A*100,'Color',col,'LineWidth',width);
    [ratio_area_min.ratio_area(j),index] =
min(A_sc./(b.^2/AR)*100);
    ratio_area_min.b(j)=b(index);
    grid on;
    xlabel('Wingspan [m]');
    ylabel('Solar Area Ratio [%]')

    if (AR == 13)
        figure(3);set(gcf,'Position',[487 204 560 420]);
        area(b,[m./m*m_pld;m./m*m_av;m_af;m_bat;m_sc;m_mppt;m_prop]');
        legend('Payload','Avionics','Airframe','Batteries','Solar
Panels','Mppt','Propulsion group','Location','NorthWest');
        xlabel('Wingspan [m]');
        ylabel('Mass [kg]');
        colormap(gray(100));
    end
end

figure(1);
plot(m_min.b,m_min.m,'xk','MarkerSize',4);
legend('8','9','10','11','12','13','14','16','18','20','Location','NorthWest');

figure(2);
subplot(2,2,1);
plot(v_min.b,v_min.v,'xk','MarkerSize',4);
subplot(2,2,4);
plot(ratio_area_min.b,ratio_area_min.ratio_area,'xk','MarkerSize',4);
legend('8','9','10','11','12','13','14','16','18','20','Location','NorthWest');

```

Appendix C.5: Stability and Control Analysis

```
%% Chris Hartney
%% Stability and Control Analysis for Solar-Powered UAV
%% Longitudinal and Directional X-Plot Program
%% Using Roskam Methods Described in Part III, V and VI

clc;
clear all;

S_h = 6:0.01:10;
S_v = 2:0.01:3;

b_wing = 5.24*3.2808399;           %% Initial Parameters
S_wing = 2.11*(3.2808399^2);      %% Dimensions are in feet
A_wing = b_wing^2/S_wing;
b_tail = 1.505*3.2808399;
S_tail = 0.2953*(3.2808399^2);
A_tail = b_tail^2/S_tail;
Cl_alpha_M_wing = 0.15;
Cl_alpha_M_tail = 0.1;
M = 0.03967;
d_f = 0.3*3.2808399;

Beta = (1-M^2)^(1/2);

k_wing = Cl_alpha_M_wing/(2*pi/Beta);
k_tail = Cl_alpha_M_tail/(2*pi/Beta);

Cl_alpha_wing = (2*pi*A_wing)/(2+((A_wing^2*Beta^2/k_wing^2)+4)^(1/2));
Cl_alpha_tail = (2*pi*A_tail)/(2+((A_tail^2*Beta^2/k_tail^2)+4)^(1/2));

k_wf = 1+0.025*(d_f/b_wing)-0.25*(d_f/b_wing)^2;

Cl_alpha_wf = k_wf*Cl_alpha_wing;

K_A = (1/A_wing)-(1/(1+A_wing^1.7));
K_lambda = 1;

l_h = 1.6105*3.2808399;
h_h = 0.003*3.2808399;
K_h = (1 - (h_h/b_wing))/((2*l_h/b_wing)^(1/3));

ep_h = 4.44*(K_A*K_lambda*K_h)^1.19;

xbar_ac_h = (227.11/40.3);
xbar_ac_wf = (66.06-0.21*40.3)/40.3;

F = 1 + ((Cl_alpha_tail*(1-ep_h)*(S_h/S_wing))/Cl_alpha_wf);
```

```

xbar_ac_A = (xbar_ac_wf + ((Cl_alpha_tail.*(1-
ep_h).*(S_h/S_wing).*xbar_ac_h)./Cl_alpha_wf))./F;

W_to = 10*2.2046;
t_rh = 0.08*0.2418*3.2808399;
W_h1 =
(3.184*(W_to^0.887)*(S_h.^0.101)*(A_tail^0.138))/(57.5*(t_rh^0.223));
xbar_cg1 = ((-
0.0129*3.2808399*0.036*2.2046+0.0381*3.2808399*0.45*2.2046+0.1962*3.280
8399*2.268*2.2046+0.4494*3.2808399*0.1*2.2046+0.4109*3.2808399*0.026*2.
2046+0.4999*3.2808399*0.015*2.2046+0.6614*3.2808399*0.01*2.2046+0.7939*
3.2808399*0.015*2.2046+0.7106*3.2808399*2.18*2.2046+0.6606*3.2808399*1.
6775*2.2046+0.9917*3.2808399*0.01*2.2046+1.0658*3.2808399*0.01*2.2046+0
.6264*3.2808399*1.955*2.2046+1.8529*3.2808399*0.6517*2.2046+W_h1*3.2808
399*2.2711)/W_to)/(0.403*3.2808399);

W_h2 = 0.4*S_h;
xbar_cg2 = ((-
0.0129*3.2808399*0.036*2.2046+0.0381*3.2808399*0.45*2.2046+0.1962*3.280
8399*2.268*2.2046+0.4494*3.2808399*0.1*2.2046+0.4109*3.2808399*0.026*2.
2046+0.4999*3.2808399*0.015*2.2046+0.6614*3.2808399*0.01*2.2046+0.7939*
3.2808399*0.015*2.2046+0.7106*3.2808399*2.18*2.2046+0.6606*3.2808399*1.
6775*2.2046+0.9917*3.2808399*0.01*2.2046+1.0658*3.2808399*0.01*2.2046+0
.6264*3.2808399*1.955*2.2046+1.8529*3.2808399*0.6517*2.2046+W_h2*3.2808
399*2.2711)/W_to)/(0.403*3.2808399);

K_N = 0.0015;
K_R1 = 1;
S_fs = 3061.5*0.00107639;
l_f = 1.2524*3.2808399;
Cn_beta_f = -57.3*K_N*K_R1*(S_fs*l_f/(S_wing*b_wing));

x_v = 1.6107*3.2808399;
Cn_beta = Cn_beta_f + Cl_alpha_tail*(S_v/S_wing)*(x_v/b_wing);
S_v(93)

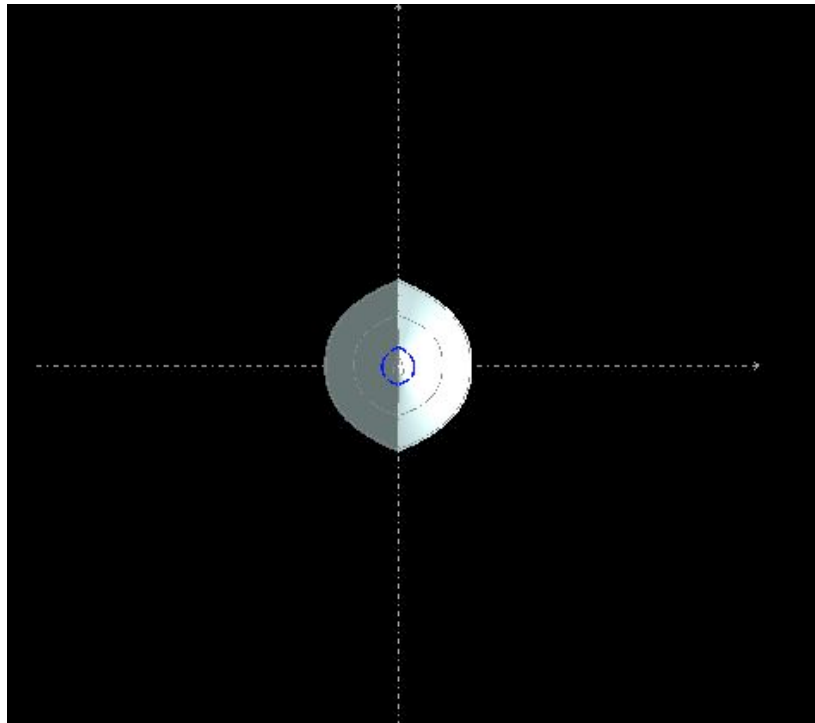
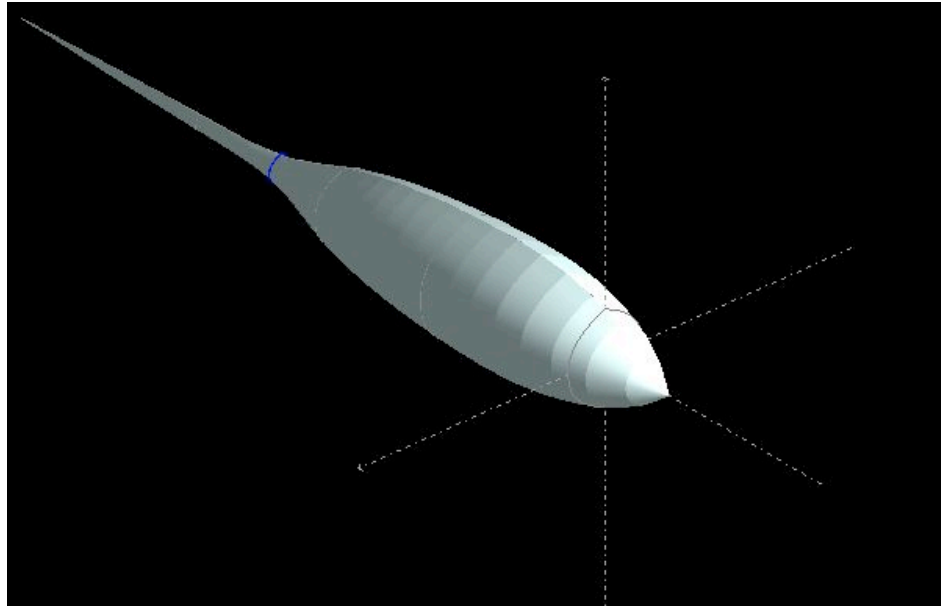
SM = xbar_ac_A - xbar_cg1;
xbar_ac_A(331);
xbar_cg1(331);
S_h(331)
figure(1);
plot(S_h, xbar_ac_A)
hold on
plot(S_h, xbar_cg1, 'r')
%%plot(S_h, xbar_cg2)
xlabel('Horizontal Stabilizer Area (in ft^2)')
ylabel('Distance from Tip of Nose (in ft per wing chord ft)')
title('Longitudinal Stability X-Plot')
legend('x_a_c_A', 'x_c_g', 'Location', 'NorthWest')

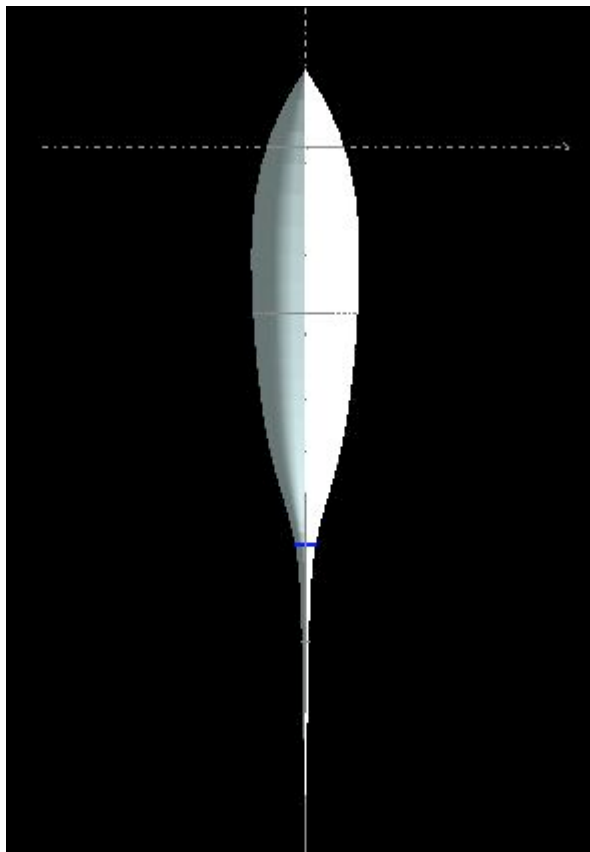
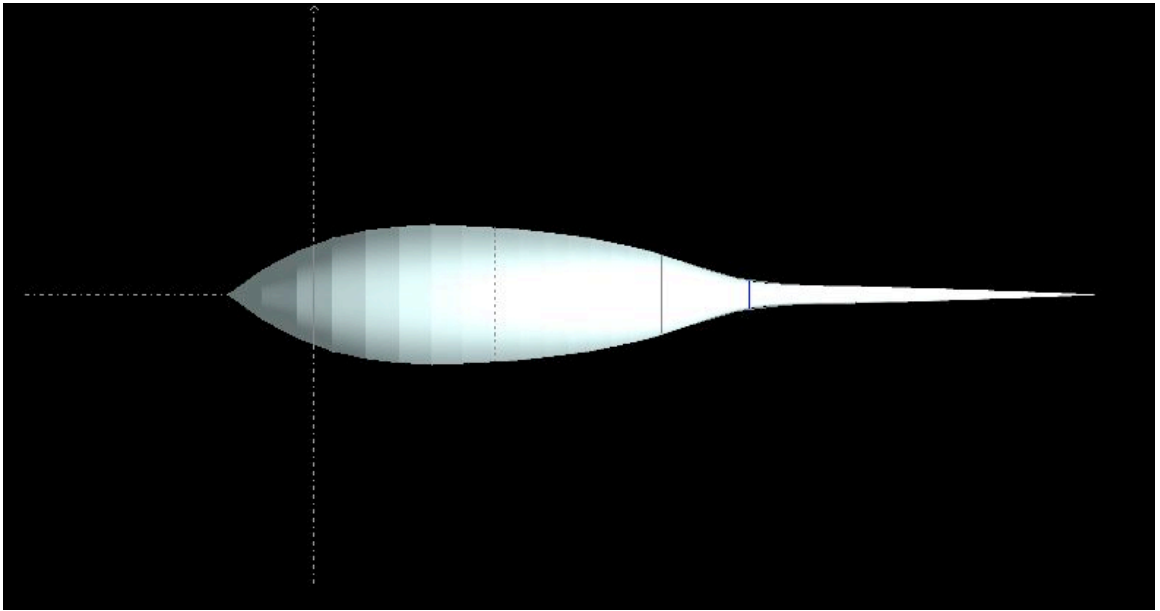
figure(2);

```

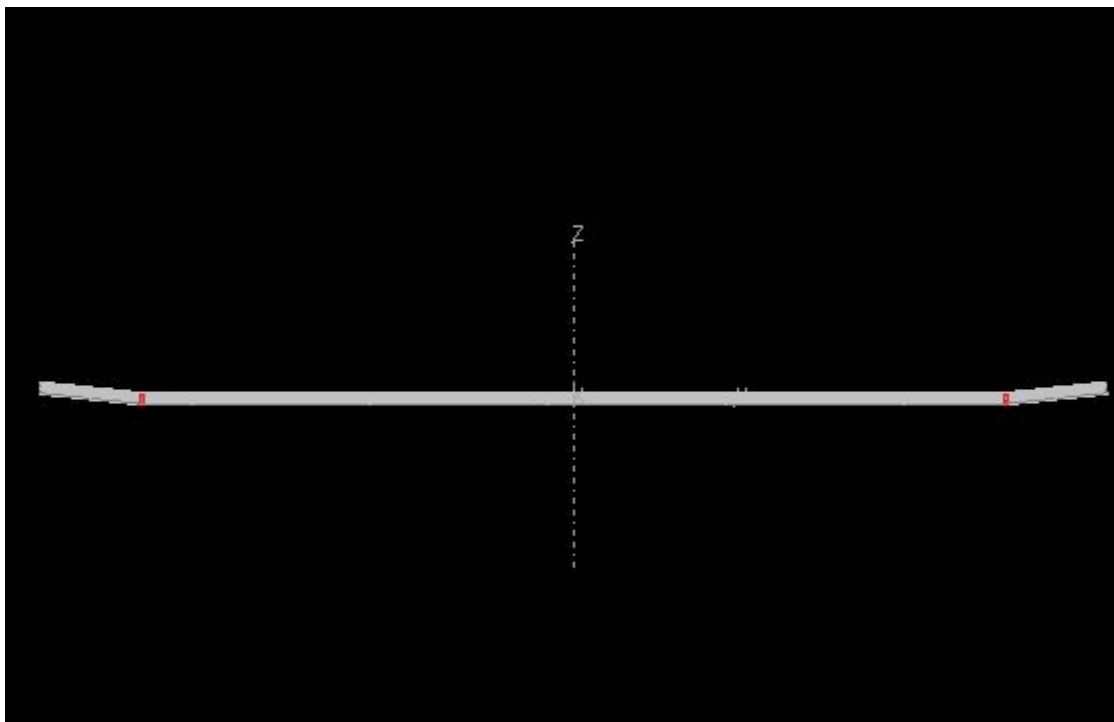
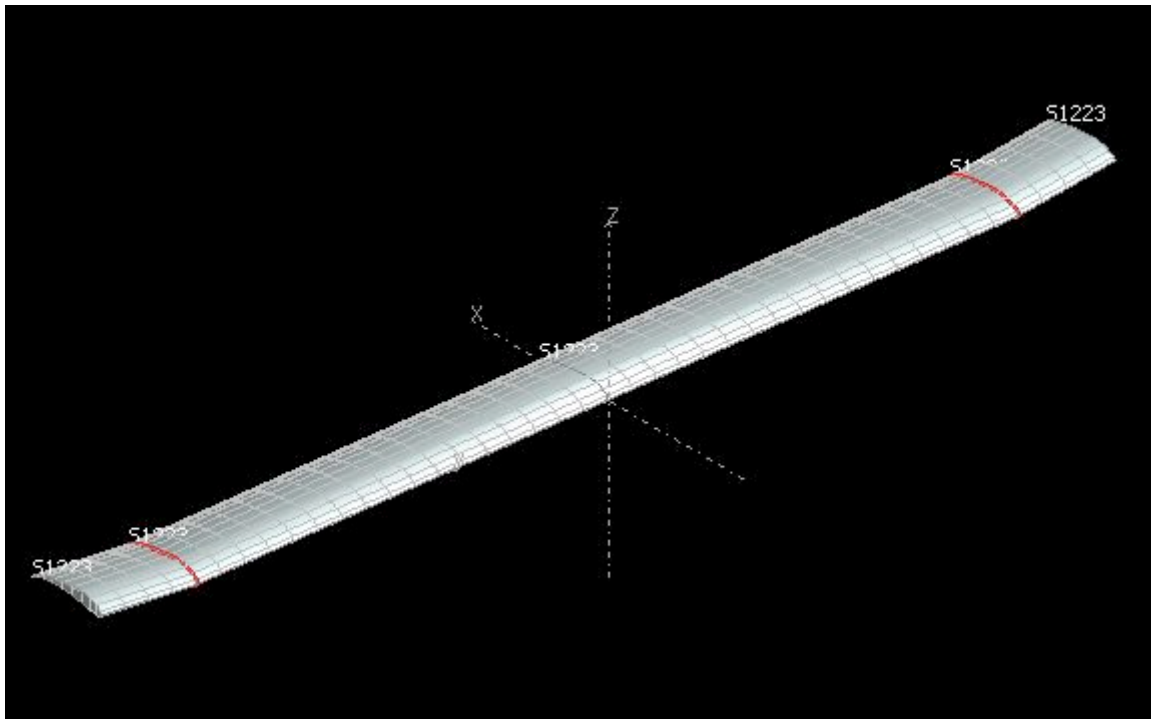
```
plot(S_v, Cn_beta)
xlabel('Vertical Stabilizer Area (in ft^2)')
ylabel('Yaw Side-slip Moment Coefficient')
title('Directional Stability X-Plot')
```

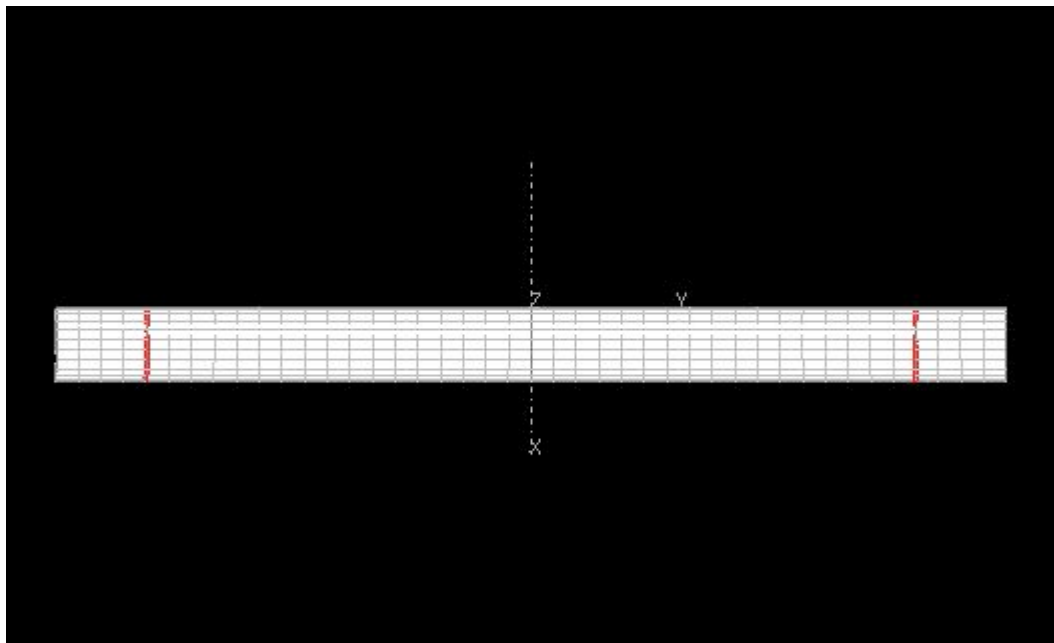
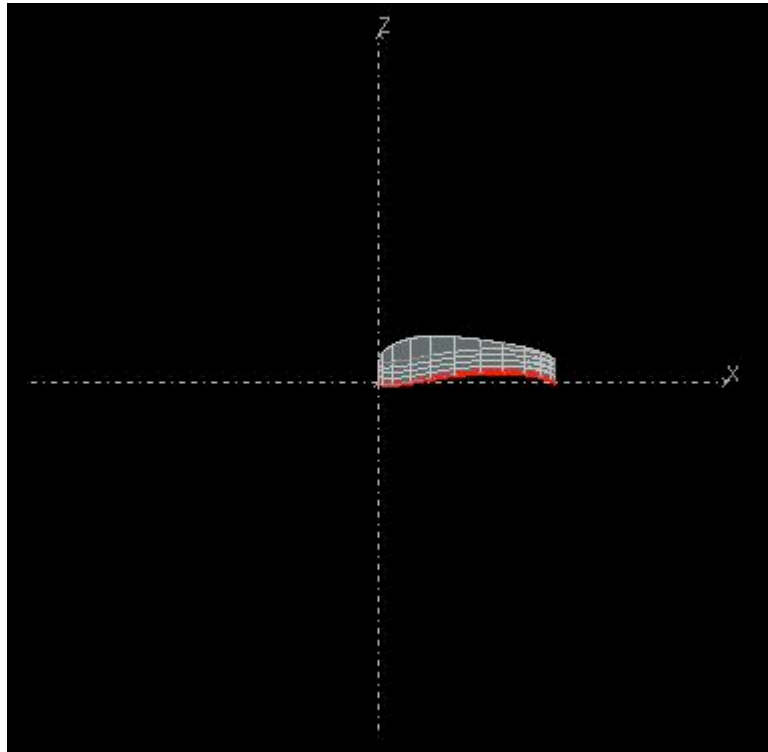
Appendix D: Fuselage Drawings



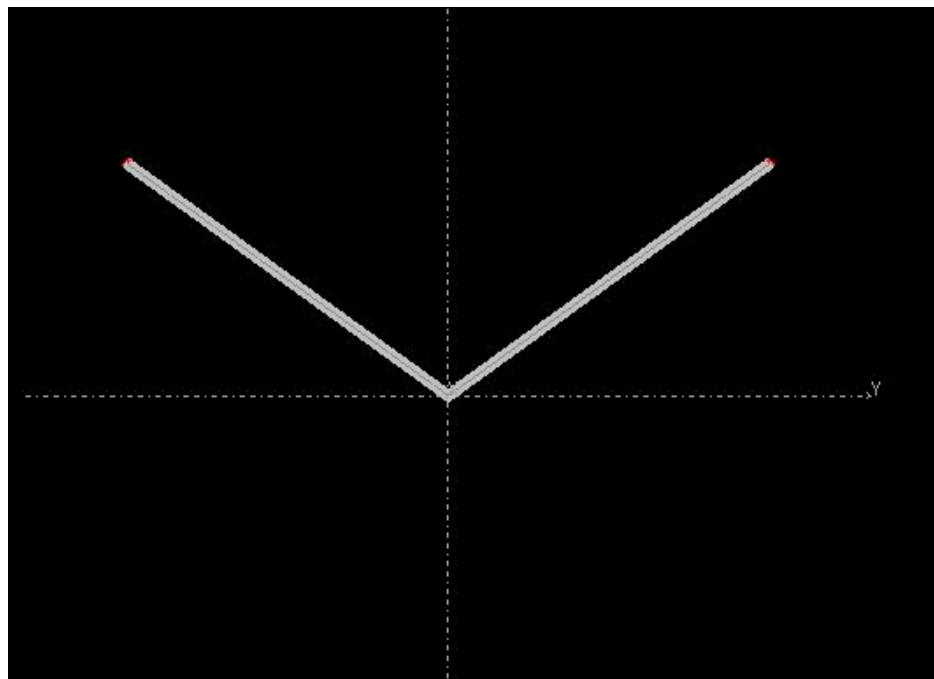
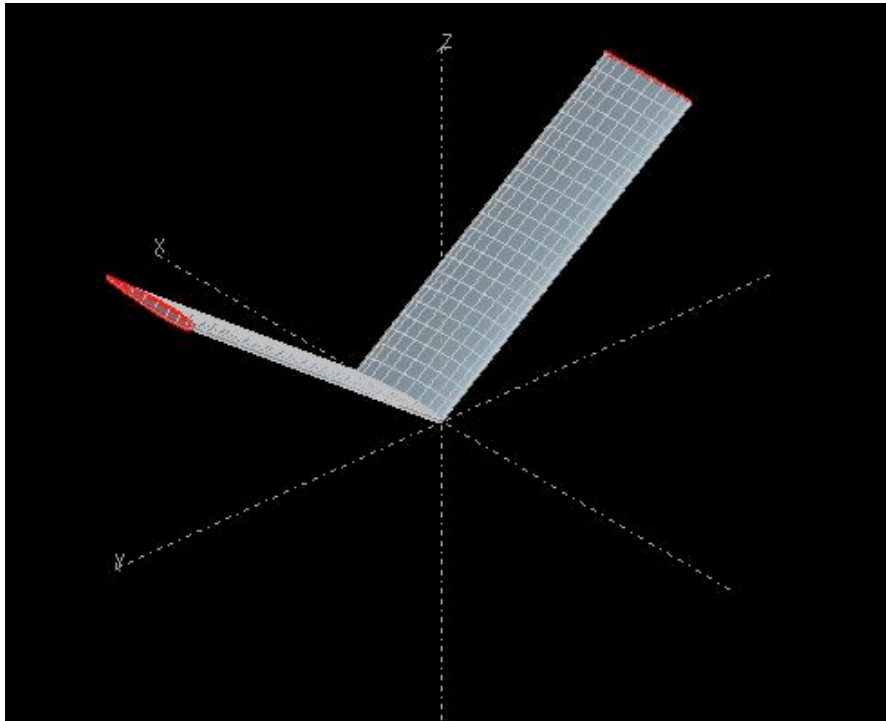


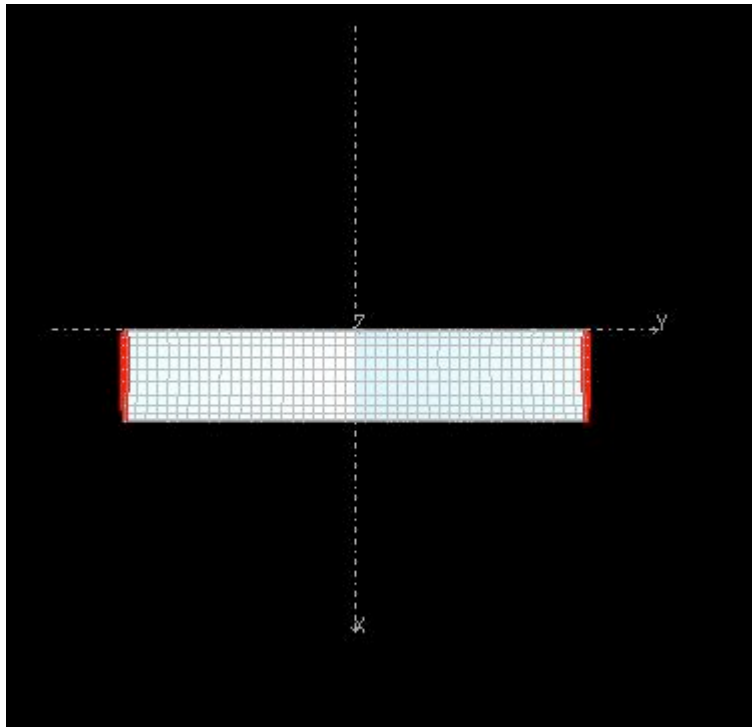
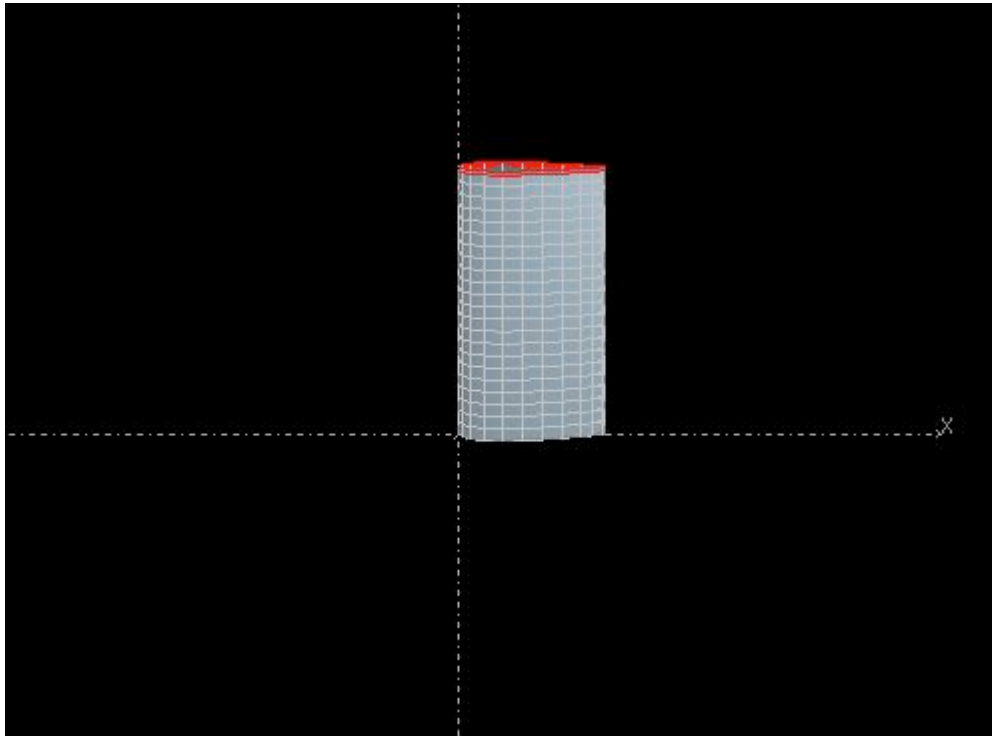
Appendix E: Main Wing Drawings



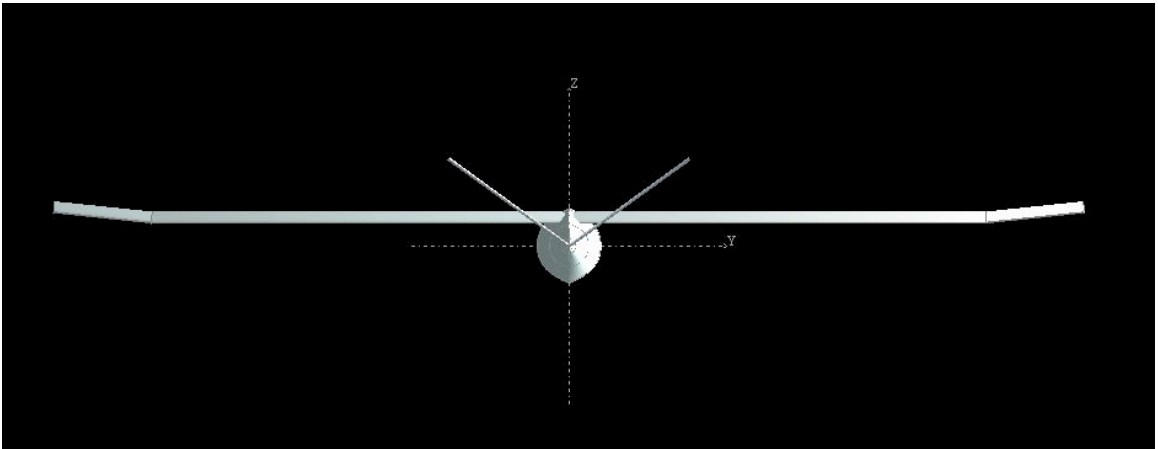
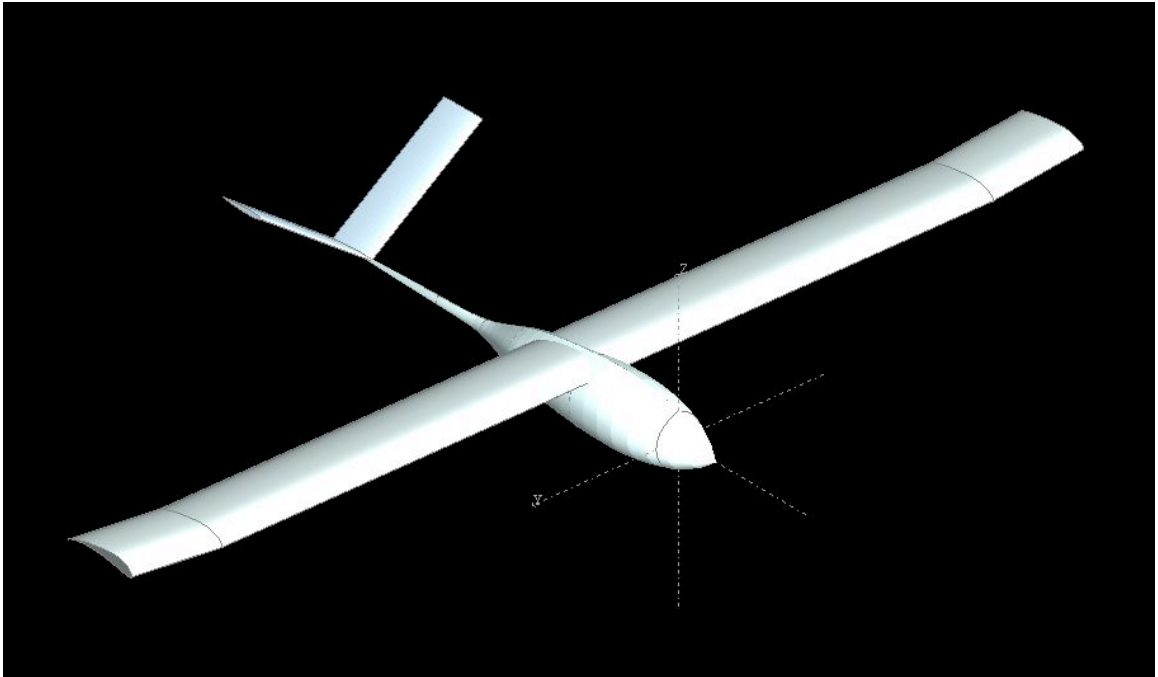


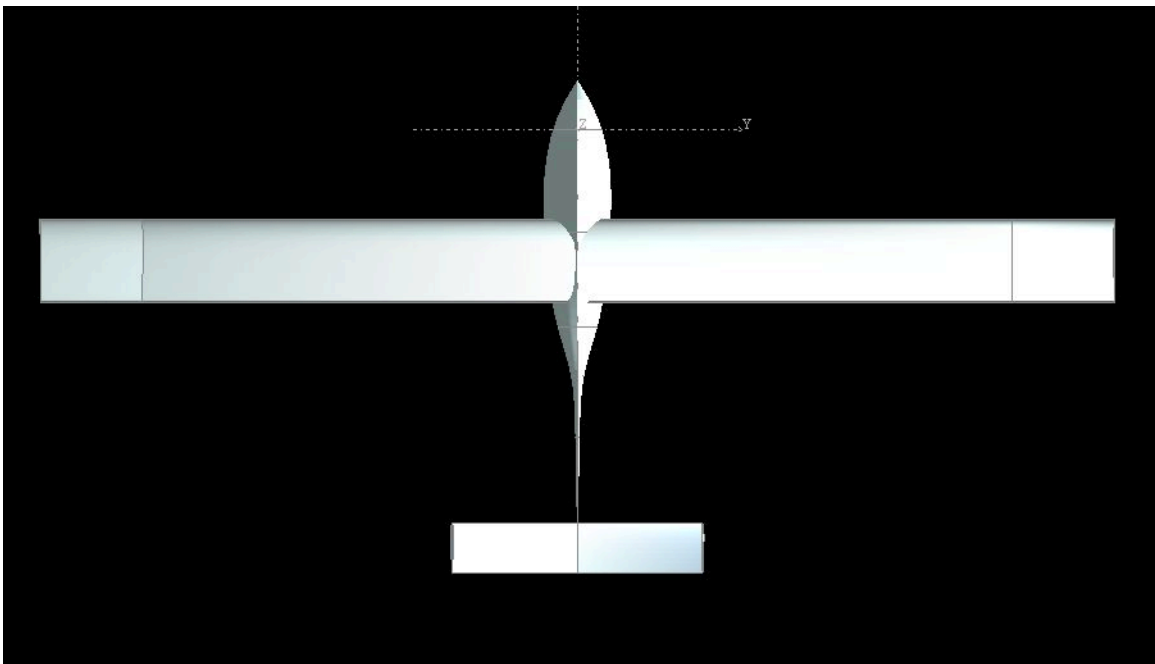
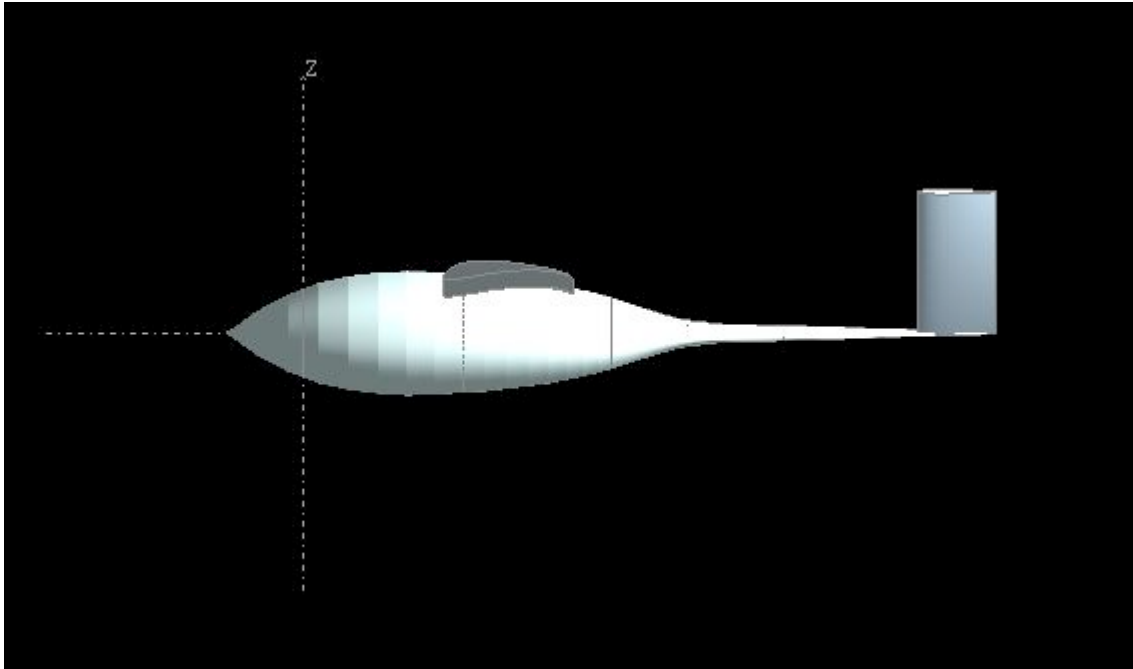
Appendix F: Empennage Drawings



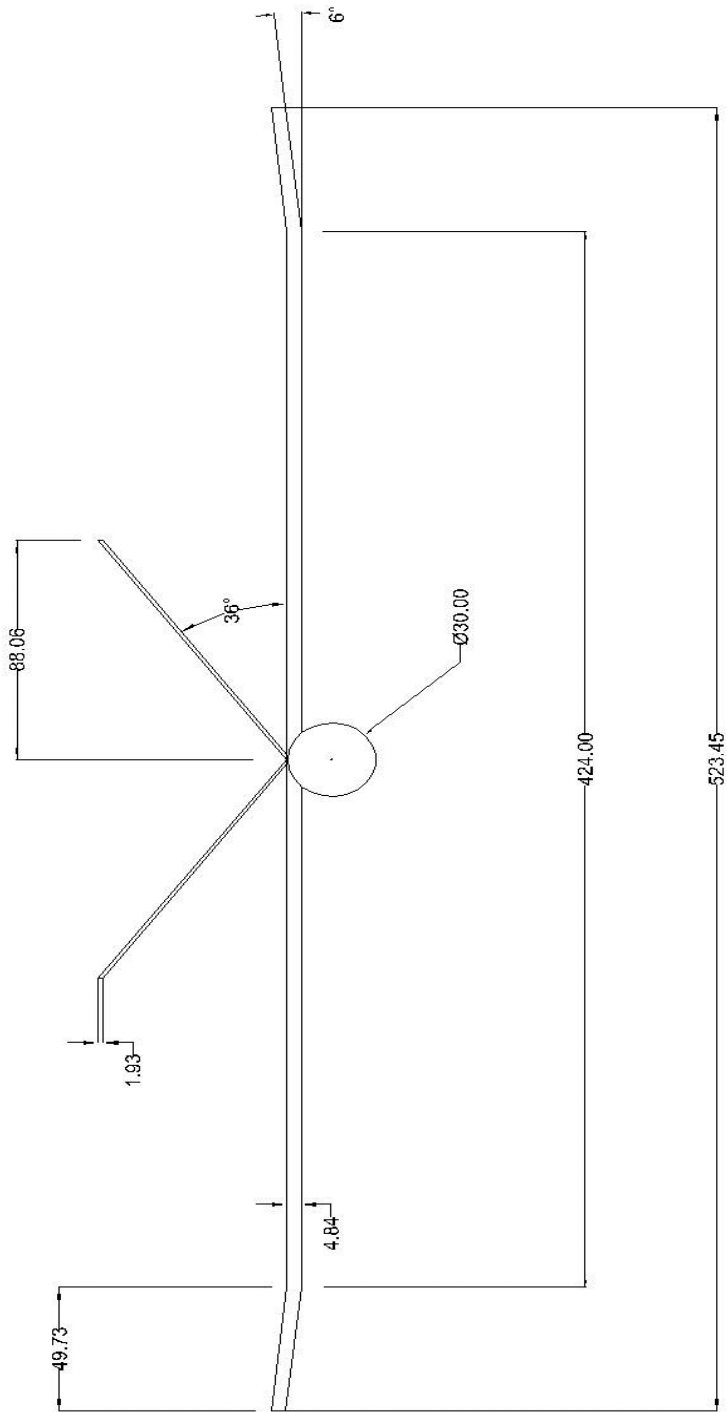


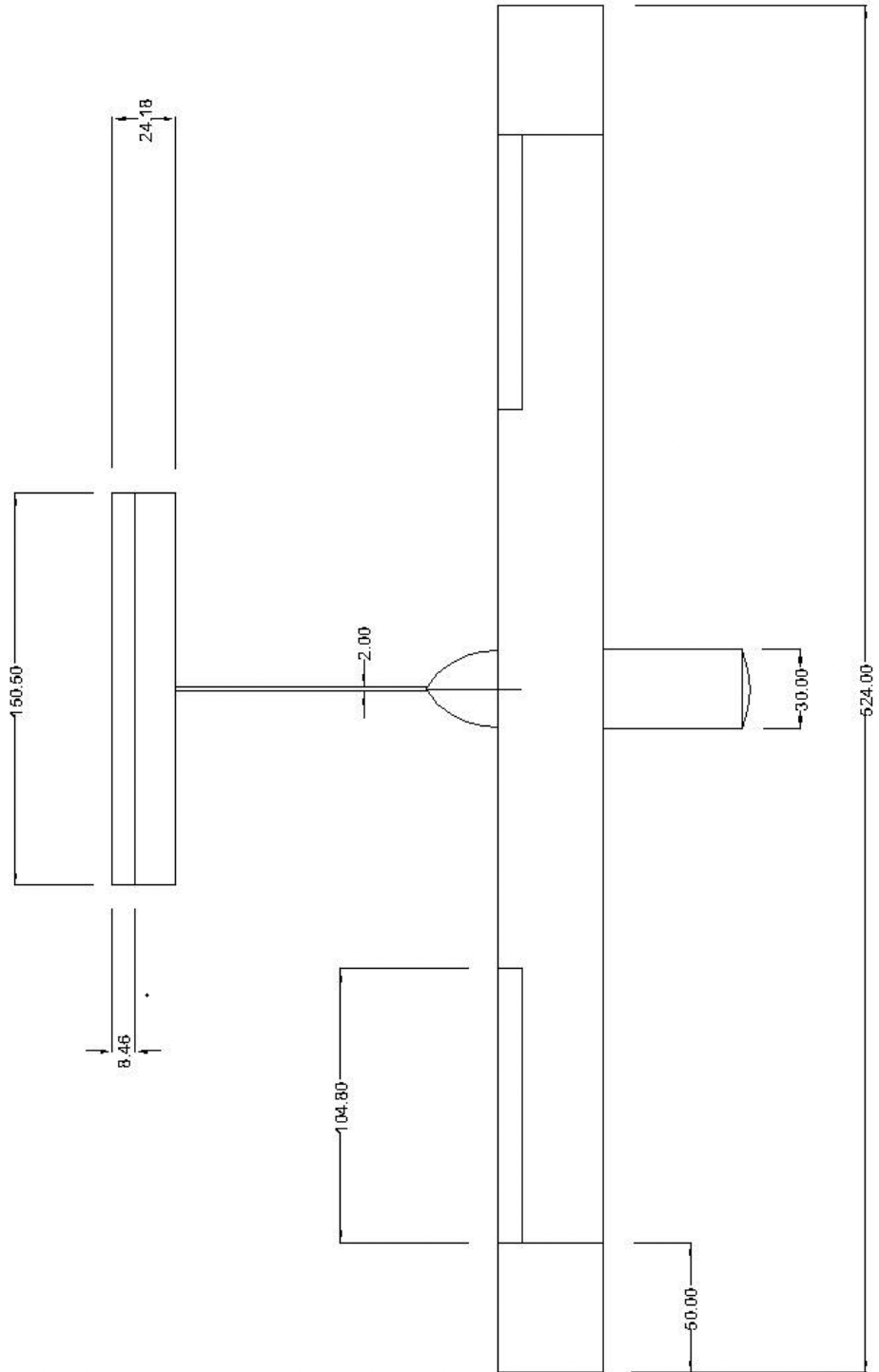
Appendix G: Main Aircraft Configuration





Appendix H: Other AutoCAD Drawings





Appendix I: XFLR5 Drag Polar Analysis

